Indo-Pacific Warming Induced by a Weakening of the Atlantic Meridional Overturning Circulation

SHANTONG SUN,[a] ANDREW F. THOMPSON,[a] SHANG-PING XIE,[b] AND SHANG-MIN LONG[c]

[a] *Environmental Science and Engineering, California Institute of Technology, Pasadena, California*
[b] *Scripps Institution of Oceanography, University of California, San Diego, La Jolla, California*
[c] *Key Laboratory of Marine Hazards Forecasting, Ministry of Natural Resources and College of Oceanography, Hohai University, Nanjing, China*

(Manuscript received 30 April 2021, in final form 24 October 2021)

ABSTRACT: The reorganization of the Atlantic meridional overturning circulation (AMOC) is often associated with changes in Earth's climate. These AMOC changes are communicated to the Indo-Pacific basins via wave processes and induce an overturning circulation anomaly that opposes the Atlantic changes on decadal to centennial time scales. We examine the role of this transient, interbasin overturning response, driven by an AMOC weakening, both in an ocean-only model with idealized geometry and in a coupled CO_2 quadrupling experiment, in which the ocean warms on two distinct time scales: a fast decadal surface warming and a slow centennial subsurface warming. We show that the transient interbasin overturning produces a zonal heat redistribution between the Atlantic and Indo-Pacific basins. Following a weakened AMOC, an anomalous northward heat transport emerges in the Indo-Pacific, which substantially compensates for the Atlantic southward heat transport anomaly. This zonal heat redistribution manifests as a thermal interbasin seesaw between the high-latitude North Atlantic and the subsurface Indo-Pacific and helps to explain why Antarctic temperature records generally show more gradual changes than the Northern Hemisphere during the last glacial period. In the coupled CO_2 quadrupling experiment, we find that the interbasin heat transport due to a weakened AMOC contributes substantially to the slow centennial subsurface warming in the Indo-Pacific, accounting for more than half of the heat content increase and sea level rise. Thus, our results suggest that the transient interbasin overturning circulation is a key component of the global ocean heat budget in a changing climate.

KEYWORDS: Meridional overturning circulation; Climate change; General circulation models

1. Introduction

The reorganization of the Atlantic meridional overturning circulation (AMOC) is typically a key feature of transitions in Earth's climate (Broecker et al. 1985). Changes in the AMOC may impact other aspects of the climate system even outside of the Atlantic basin, with particular attention paid to the coupling between the AMOC and the Southern Ocean in previous studies (e.g., Stocker and Johnsen 2003; Marshall and Speer 2012; Sun et al. 2020a). Zonal changes in ocean heat content in response to a changing AMOC, on the other hand, have received less attention. Here we propose that changes in the AMOC result in a redistribution of heat between the Atlantic and Indo-Pacific basins through a transient interbasin overturning circulation, and in the case of a weakening AMOC, can produce a centennial-scale subsurface warming in the Indo-Pacific (Fig. 1).

Interbasin pathways that connect the Atlantic and Indo-Pacific Oceans are well established (Gordon 1986; Talley 2013; Newsom and Thompson 2018), but only recently has the transient adjustment of this interbasin overturning circulation, in response to AMOC changes, been explored (Sun et al. 2020b). A weakened AMOC is associated with a reduced formation rate of North Atlantic Deep Water (NADW) that modifies the density structure in the North Atlantic (e.g., Jansen et al. 2018). These changes propagate as Kelvin waves southward along the western boundary, eastward along the equator, and then poleward along the eastern boundary in the Atlantic (Huang et al. 2000; Johnson and Marshall 2004; Cessi et al. 2004) and cause a change in the isopycnal depth on the eastern boundary of the South Atlantic. Thus, a reduction in the AMOC strength is characterized by an anomalous southward, geostrophically balanced, upper-ocean volume transport that is established within months. The signal of isopycnal depth changes propagates farther eastward around South Africa, via coastal Kelvin waves, into the Indo-Pacific basins, leading to a similar geostrophically balanced overturning response that is characterized by an anomalous northward, upper-ocean volume transport and a reduced upwelling (cf. Sen Gupta et al. 2016). Thus, the Indo-Pacific overturning changes substantially oppose the Atlantic changes (black dashed arrows in Fig. 1).

These overturning circulation perturbations may also impact heat transport and heat content within each basin. The meridional heat transport anomaly (H') caused by overturning circulation changes (ψ') in a basin, defined in Eulerian depth space, can be expressed as

$$H'_{\text{Eulerian}} = -\rho_0 c_p \int_{-z_{\text{bot}}}^{0} \frac{\partial \psi'}{\partial z} \bar{\theta} dz, \tag{1}$$

where ρ_0 is seawater density, c_p is seawater specific heat capacity, $\bar{\theta}$ is the time and zonal-mean potential temperature

Supplemental information related to this paper is available at the Journals Online website: https://doi.org/10.1175/JCLI-D-21-0346.s1.

Corresponding author: Shantong Sun, shantong@caltech.edu

DOI: 10.1175/JCLI-D-21-0346.1

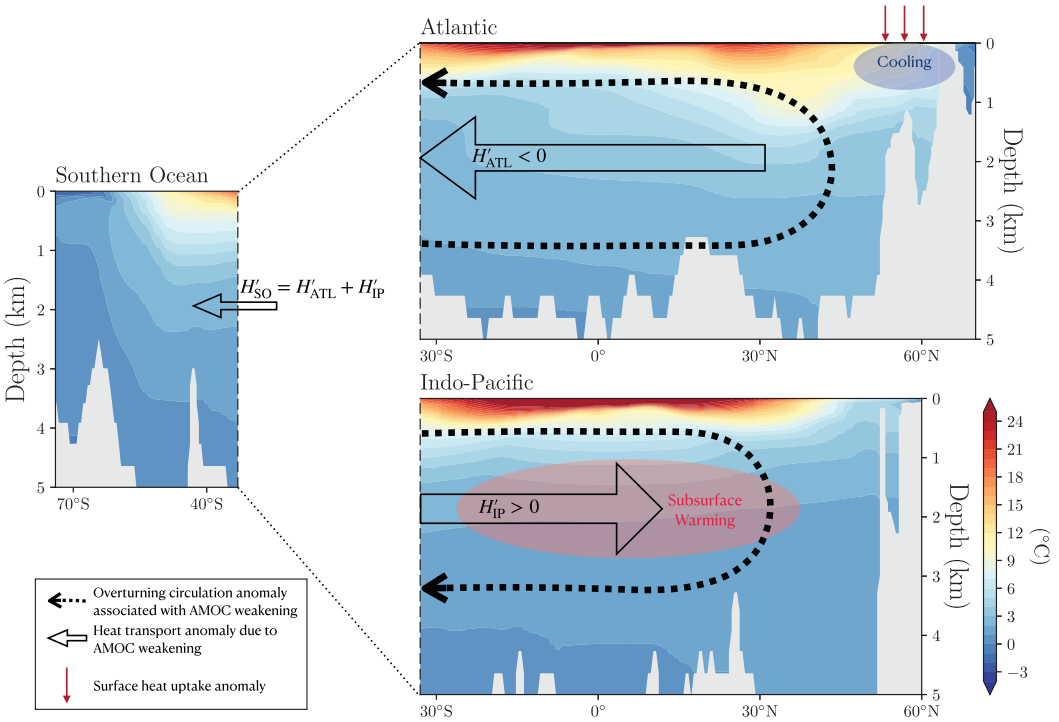

FIG. 1. Schematic of overturning circulation and heat transport responses to a weakening of the AMOC, assuming no change in atmospheric state. The background color shows potential temperature along (left) 170°W in the Southern Ocean, (top right) 20°W in the Atlantic, and (bottom right) 170°W in the Indo-Pacific from the ECCO state estimate (Forget et al. 2015). The thick black dashed lines with arrow represent the overturning circulation anomaly following a weakening of the AMOC. The black hollow arrow shows the heat transport anomaly due to overturning circulation changes. On decadal to centennial time scales, the Indo-Pacific overturning circulation substantially compensates the AMOC changes, leading to a heat transport response with opposing directions in the Atlantic ($H'_{ATL} < 0$) and Indo-Pacific ($H'_{IP} > 0$) basins. The interbasin heat redistribution causes a cooling in the high-latitude North Atlantic and a warming in the subsurface Indo-Pacific. The heat transport into the Southern Ocean, $H'_{SO} = H'_{ATL} + H'_{IP}$, is a small residual of the northern basin transport anomalies on decadal to centennial time scales and slowly intensifies on multicentennial time scales, based on the MITgcm ocean-only simulations (section 3).

in the control climate and contributions to the heat transport anomaly due to temperature changes have been neglected (section 5a), z_{bot} is the depth of the seafloor, and ψ' is the Eulerian-mean overturning circulation streamfunction anomaly. This last term (ψ') is defined as the vertical integral of the meridional velocity anomaly v', the deviation away from the control climate, also integrated from the western boundary (x_w) to the eastern boundary (x_e). The combination of a weakened AMOC and the vertical distribution of temperature (warmer at the surface) suggests a southward heat transport anomaly in the Atlantic ($H'_{ATL} < 0$) and a northward heat transport anomaly in the Indo-Pacific ($H'_{IP} > 0$) (black hollow arrows in Fig. 1). The divergence and convergence of heat transport following a weakening in AMOC strength leads to a cooling in the high-latitude North Atlantic and a warming in the Indo-Pacific, respectively, suggesting a zonal redistribution of heat between the Atlantic and Indo-Pacific basins by the transient interbasin overturning circulation (Fig. 1).

Climate models consistently project the AMOC strength to decline in the twenty-first century due to surface warming and freshening in the North Atlantic (Cheng et al. 2013; Weijer et al. 2020). Many previous AMOC studies have highlighted the impacts local to the Atlantic Ocean (e.g., Xie and Vallis 2012; Winton et al. 2013; Liu et al. 2020). For example, a weakening of the AMOC in a warming climate reduces the northward ocean heat transport in the Atlantic basin, leading to a cooling of the high-latitude North Atlantic that resembles the North Atlantic warming hole (Menary and Wood 2018). This ocean cooling reduces the atmosphere–ocean temperature difference and leads to an enhanced anthropogenic surface heat uptake in the high-latitude North Atlantic ocean (red arrow in Fig. 1) (e.g., Garuba and Klinger 2016; Shi et al. 2018).

In this study, we focus on heat transport and heat content changes that are responses to AMOC perturbations but occur in regions remote from the Atlantic basin. Specifically, we attribute a slow centennial-scale subsurface warming of the Indo-Pacific to an interbasin heat transport. Increasing atmospheric CO_2 levels produce ocean warming on two distinct time scales: a fast response, occurring over several years, due

to increases in the ocean's mixed layer temperature; and a slow response, occurring over centuries to millennia, due to warming of the deep ocean (Stouffer 2004; Held et al. 2010). By subtracting the global-mean temperature profile after the fast response in a 1% CO_2 experiment, Long et al. (2014) show that the global-mean slow warming is characterized by a prominent subsurface warming. Traditionally, this subsurface warming signature has been attributed to a diffusive mixing that fluxes heat between the surface and the subsurface ocean (e.g., Gregory 2000; Held et al. 2010; Wang et al. 2015), a mechanism that relies on diabatic processes. Instead, we argue that a transient interbasin overturning circulation, which is largely associated with an adiabatic movement of isopycnals (Sun and Thompson 2020, their Fig. 3b), can also contribute substantially to the slow subsurface warming in the Indo-Pacific basins.

Interbasin exchange may also explain other aspects of heat content changes in individual basins. For example, Shatwell et al. (2020) recently used a suite of idealized climate model simulations to discuss the influence of the AMOC weakening on ocean warming. Their results showed that the Indo-Pacific warms at approximately the same rate as the Atlantic in response to an abrupt CO_2 doubling, despite a larger surface heat uptake rate per unit surface area in the Atlantic basin. Here we suggest that the similar warming rate between the Indo-Pacific and Atlantic is actually due to the heat content redistribution between these two basins by the transient interbasin overturning circulation, driven by the AMOC weakening. This redistribution was not considered in Shatwell et al. (2020).

Modifications to the Atlantic meridional heat transport, associated with transitions in the AMOC, have also been identified as key features of abrupt climate change throughout Earth's history. In particular, these processes have been linked to an oceanic thermal bipolar seesaw between the North Atlantic and the Southern Ocean that occurs over millennial time scales in glacial and deglacial periods (e.g., Stocker and Johnsen 2003; Barker et al. 2009). Ice core records from Greenland suggest that variability in Northern Hemisphere (NH) climate was dominated by Dansgaard–Oeschger (DO) events throughout the last glacial period. DO events are characterized by large and abrupt fluctuations in temperature in the NH (Dansgaard et al. 1993) that are accompanied by temperature changes of the opposite sign in the Southern Hemisphere (SH). However, in contrast to the abrupt temperature changes in the NH, temperature variations over Antarctica were more gradual and approximately out of phase with the north (Blunier and Brook 2001; Barker et al. 2009). This antiphasing relationship in temperature changes between Greenland and Antarctica has been linked to changes in the AMOC (e.g., Stocker and Johnsen 2003; Liu et al. 2009). In this paradigm, a surface forcing perturbation in the North Atlantic weakens the AMOC and reduces Atlantic northward heat transport [Eq. (1)], leading to a cooling in the high-latitude North Atlantic and warming in the SH. Stocker and Johnsen (2003) suggested that the Southern Ocean acts as a heat reservoir and the slower change in SH temperature occurs due to a diffusive coupling of the Southern Ocean heat storage with the reduced AMOC. They argued that this gives rise to a 1000-yr time scale for SH changes although this value is empirical in their study. Again, invoking interbasin heat exchange provides a more physical explanation for this behavior. More concretely, the gradual rate of Antarctica temperature change, in comparison to abrupt NH changes, occurs because much of the reduced northward Atlantic heat transport related to AMOC modifications is compensated by a northward heat transport anomaly in the Indo-Pacific, caused by a transient interbasin overturning circulation on centennial time scales. The heat transport into the Southern Ocean, which governs the temperature variations recorded in Antarctic ice cores (Markle et al. 2017), arises from the residual between the Atlantic and Indo-Pacific heat transport. This residual is considerably weaker than the basin heat transports and only becomes significant on multicentennial to millennial time scales, determined by the adjustment time scales of the Southern Ocean overturning circulation (Thompson et al. 2019; Sun et al. 2020b).

The goal of this study is to illustrate the magnitude and structure of the heat redistribution carried out by the transient interbasin overturning circulation and to examine its role in ocean temperature variations in a changing climate. The structure of the paper is as follows. In section 2, we introduce two separate model frameworks, ocean-only and coupled simulations, as well as the diagnostic techniques that we apply in this study. We diagnose and explain the interbasin heat transport due to AMOC changes in section 3. We compare the dynamics in the ocean-only model to the behavior of the interbasin exchange in a coupled model and connect the interbasin heat transport to a slow warming in the Indo-Pacific in response to an increased CO_2 forcing in section 4. A discussion of the results is provided in section 5, followed by a brief summary in section 6.

2. Approach and methodology

Our approach is to use a hierarchy of numerical models to illustrate the dynamics of interbasin heat transport and its climate impacts. We start with ocean-only simulations to isolate the relationships between basin-scale overturning circulations and heat transports. Yet, the ocean-only model omits a number of key components of the climate system, including feedbacks between the atmosphere and ocean. To account for these limitations, we next analyze output from a coupled model and assess the relative importance of interbasin heat transport as compared to surface heat uptake on ocean warming under increased CO_2 radiative forcing.

a. Ocean-only simulations

We use the Massachusetts Institute of Technology General Circulation Model (MITgcm; Marshall et al. 1997) to carry out ocean-only simulations that use a nonlinear equation of state (Jackett and Mcdougall 1995). The model domain, discretized on a 1°-resolution grid, includes three idealized basins that represent the Atlantic, Indian, and Pacific Oceans, connected in the south with a reentrant channel that

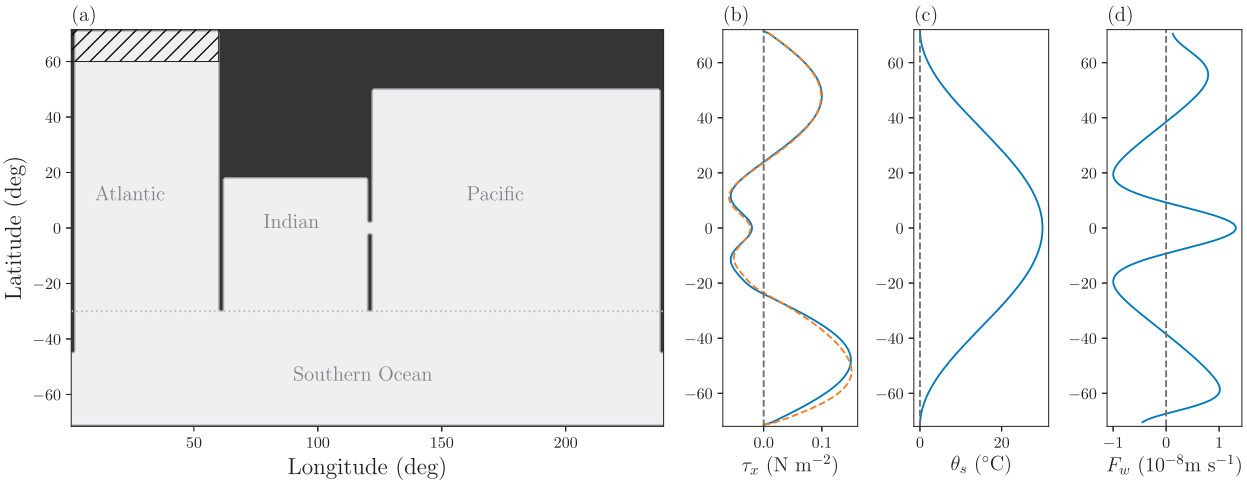

FIG. 2. Model configurations for the MITgcm ocean-only simulations. (a) Geometry of the model domain. The ocean is 4000 m deep everywhere except for a 2500-m-deep submarine sill in the Southern Ocean that represents Drake Passage. The black shading represents continents. The hatched area indicates the region where the 0.05-Sv freshwater hosing is applied. Surface forcing applied to the model: (b) zonal wind stress τ_x (blue; N m^{-2}), (c) restoring surface temperature θ_s (°C), and (d) freshwater flux F_w (m s^{-1}). The orange dashed line in (b) represents a wind stress forcing with southward-shifted Southern Hemisphere westerlies that mimic the CCSM4 abrupt 4xCO_2 experiment, as discussed in text S2 of the supplemental material.

represents the Southern Ocean (Fig. 2a), which is a similar domain to the reduced gravity model in Sun and Thompson (2020). In the vertical, there are 30 vertical layers ranging from 20 m at the top to 250 m at the bottom. A vertical diffusivity is implemented that is a function of depth and increases from 2.0×10^{-5} m^2 s^{-1} at the surface to 1.0×10^{-4} m^2 s^{-1} with a transition depth of 2000 m (Bryan and Lewis 1979). Vertical convection is represented by an implicit diffusion with a diffusivity of 10 m^2 s^{-1}, whenever the stratification is hydrostatically unstable. Unresolved eddies are represented using the skew-flux form of the Gent–McWilliams (GM) parameterization with an eddy thickness diffusivity K_{GM} = 500 m^2 s^{-1}. Isopycnal diffusion due to eddies are represented using the Redi scheme with K_{Redi} = 500 m^2 s^{-1} (Redi 1982). The momentum is dissipated via Laplacian viscosity, biharmonic viscosity, and vertical viscosity with coefficients A_h = 1.0×10^4 m^2 s^{-1}, $A_4 = 1.0 \times 10^{12}$ m^4 s^{-1}, and $A_v = 1.0 \times 10^{-3}$ m^2 s^{-1}, respectively.[1] The biharmonic viscosity is used to suppress grid-scale noise.

The model is forced with a zonally uniform zonal wind stress (blue curve in Fig. 2b). Temperature (θ) at the surface is restored to a prescribed zonally uniform temperature profile (Fig. 2c) with a relaxation time scale of 20 days (cf. Haney 1971). For the salinity surface boundary condition, we use a prescribed freshwater flux F_w (Fig. 2d) that is uniform in the zonal direction except in the Pacific Ocean, where an extra constant freshwater flux of 0.3×10^{-8} m s^{-1} is added to suppress convection in the high-latitude North Pacific. To avoid possible bistability due to the mixed surface boundary conditions (Stommel 1961), we also relax the surface salinity to a constant, 35 g kg^{-1}, on a time scale of 2 years (cf. Griffies et al. 2009).

We run the model for 3000 years, at which point the model reaches an approximate steady state, as determined by changes in the AMOC strength. We take the steady-state simulation as a control ("Control") and then apply a 0.05 Sv (1 Sv ≡ 10^6 m^3 s^{-1}) freshwater hosing in the North Atlantic (hatched area in Fig. 2a) to perturb the AMOC. The simulation is run for another 250 years ("Hosing"), during which the freshwater hosing is kept constant. We compare the differences in the volume and heat transports as well as heat content between the control and perturbation runs due to freshwater hosing. We note that the hosing experiment is only intended to show the oceanic response to AMOC perturbations, such as in a warming climate or during DO events; the simulations are not designed to reproduce comprehensive climate responses given that the model omits key components of the climate system.

b. *Coupled simulations*

The AMOC is projected to decline in response to anthropogenic greenhouse gas forcing. To evaluate the interbasin heat redistribution and its impact on basin-scale temperature changes related to a modified AMOC in a future, warming climate, we examine an abrupt CO_2 quadrupling (4xCO_2) experiment. Specifically, we make use of the NCAR Community Climate System Model, version 4 (CCSM4; Gent et al. 2011), which is part of phase 5 of the Coupled Model Intercomparison Project (CMIP5; Taylor et al. 2012). The CCSM4 4xCO_2 experiment, with realistic geography, is initialized from an approximately equilibrated CCSM4 preindustrial run at year 1850, but with the atmospheric CO_2 level instantaneously

[1] Note that the description of the model in Sun et al. (2020b) stated $A_h = 1.0 \times 10^{-4}$ m^2 s^{-1}, but the actual value used was A_h = 1.0×10^4 m^2 s^{-1}.

quadrupled. Both the preindustrial and the 4xCO_2 simulations are continued from 1850 for another 250 years. In the following analysis, we focus on the differences between the preindustrial and 4xCO_2 runs.

c. Model diagnostics

The isopycnal overturning circulation streamfunction Ψ is used to represent the meridional overturning circulation and to define the overturning-driven heat transport (see the appendix). The streamfunction Ψ, defined in isopycnal coordinates, accounts for contributions due to both transient and standing eddies, and it is considered to be a more accurate description of the overturning circulation than the overturning circulation streamfunction defined in depth space (Viebahn and Eden 2012; Ballarotta et al. 2013), which is typically used in the climate literature. The Eulerian-mean streamfunction [Eq. (A3)], defined in depth space, is generally an acceptable approximation of the overturning circulation in the low and midlatitudes, but it can significantly misrepresent the overturning circulation in the high latitudes, including the Southern Ocean and the subpolar North Atlantic, even after accounting for transient eddies. As such, the magnitude of the heat transport associated with the Eulerian-mean overturning circulation [Eq. (1)] is usually smaller than the heat transport associated with the isopycnal overturning circulation [Eq. (A4)].

Changes in the basin-scale heat content ($\mathscr{T}$; J) can be attributed to anomalies in three different physical processes (assuming a closed northern boundary): (i) surface heat uptake (H_{sfc}), (ii) lateral heat transport across the southern boundary due to the overturning circulation (H_{OT}), and (iii) additional lateral processes due to gyre circulation and eddy diffusion processes (H_R), that is,

$$\mathscr{T}'(t) = \int_0^t \left[H'_{\text{sfc}}(t) + H'_{\text{OT}}(t) + H'_{\text{R}}(t)\right]dt, \tag{2}$$

where the prime represents a deviation from the control run, and the heat transport terms H have units of watts. The estimate of the heat transport by the overturning circulation H_{OT} in Eq. (A4) also includes contributions from the subtropical cell, which is associated with the wind-driven gyre circulation and projects to density/depth space as a shallow overturning circulation (upper 500 m in Figs. 3b,c).

In a changing climate the range of density classes and the ocean's vertical stratification differ substantially between the control and perturbed states, and it becomes challenging to isolate heat transport contributions due to circulation changes in isopycnal coordinate (see further discussion in sections 3 and 4). Therefore, calculations in Eulerian depth space are used to determine the evolution of the ocean's vertical temperature distribution due to circulation changes [Eqs. (3)–(7) in section 3b]. We remind the reader that this Eulerian-depth approach typically results in an underestimation of the heat transport associated with the overturning circulation.

3. Interbasin heat redistribution due to AMOC perturbations

In this section, we present results from the MITgcm ocean-only simulations.

a. Transient interbasin overturning circulation

In the Control simulation at equilibrium, the overturning circulation in the Atlantic basin is primarily connected to the Southern Ocean through a pole-to-pole overturning circulation (Figs. 3a–c). In other words, the majority of NADW, formed in the high-latitude North Atlantic and carried southward by the AMOC, rises to the surface in the Southern Ocean along isopycnals via adiabatic upwelling, where it is transformed to other density classes (Wolfe and Cessi 2011; Marshall and Speer 2012). In contrast, the overturning in the Indo-Pacific basins is mainly characterized by an anticlockwise cell, associated with a northward flow of Antarctic Bottom Water (AABW) close to the seafloor, transformation into lighter water by interior diapycnal mixing, and a southward return flow at shallower depths.

In response to the 0.05-Sv freshwater hosing perturbation, the AMOC both weakens in strength and shoals in depth (Fig. 3e). The AMOC strength at 30°S, defined as the maximum value of the annual-mean AMOC streamfunction at this latitude, weakens by ~20% over the first 50 years and then remains roughly stable afterward (gray line in Fig. 4a). This 50-yr time scale of AMOC weakening is associated with the gyre spinup/spindown dynamics in the North Atlantic, in response to the freshwater perturbation, and is determined by the transit time of Rossby waves across the Atlantic basin (Sun et al. 2020b). There is also a slow millennial-scale evolution of the overturning circulation that is associated with the adjustment of the deep stratification, which is not resolved in the 250-yr simulation (cf. Jansen et al. 2018; Sun et al. 2020b).

Unlike the steady-state balance, the AMOC weakening that occurs during the 250-yr simulation is largely decoupled from the Southern Ocean, where the overturning circulation remains relatively unchanged, as found in Sun et al. (2020b) (Figs. 3d,e). Instead, AMOC changes are principally compensated by overturning circulation anomalies in the Indo-Pacific basins (Figs. 3e,f). The Indo-Pacific overturning response is characterized by a northward transport anomaly in the upper 1.8 km and a southward transport anomaly in the abyss, leading to a volume transport convergence anomaly in the upper Indo-Pacific that is largely balanced by an adiabatic deepening of the isopycnals (Sun and Thompson 2020). This isopycnal deepening results in a subsurface warming through the heave effect (Purkey and Johnson 2013), as discussed in the next subsection.

We quantify the meridional volume transport across 30°S within the upper 1 km, which carries the upper, northward-flowing branch of AMOC (gray and blue lines in Fig. 4a), in the Atlantic and the Indo-Pacific basins. The anomalous northward volume transport in the upper Indo-Pacific largely cancels the anomalous southward transport in the Atlantic Ocean. The approximately synchronous, but opposite, responses between the Atlantic and Indo-Pacific are due to

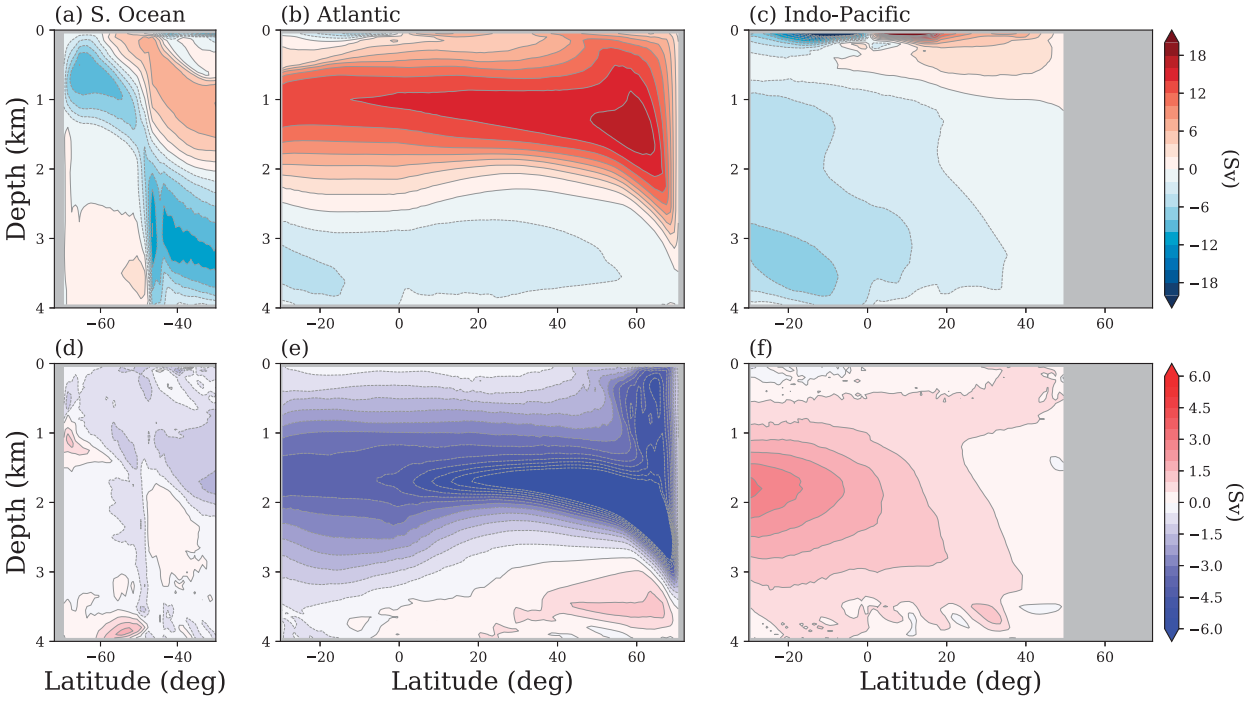

FIG. 3. Isopycnal overturning circulation in the MITgcm simulations, mapped to depth coordinate (see details in the appendix). (a)–(c) Meridional overturning circulation streamfunction in the Control simulation, averaged over the last 50 years. (d)–(f) Changes in the overturning circulation due to freshwater hosing, calculated as the difference in overturning circulation streamfunction of the Hosing run from Control, averaged over the last 50 years. "S. Ocean" stands for "Southern Ocean." Positive and negative values indicate clockwise and anticlockwise overturning circulations, respectively.

the fast propagation of coastal Kelvin waves. The residual between the Atlantic and Indo-Pacific volume transports (orange line in Fig. 4a) denotes changes in the Southern Ocean overturning circulation, which responds on multicentennial time scales, as discussed in Sun et al. (2020b).

b. *Interbasin heat redistribution and subsurface Indo-Pacific warming*

The transient, interbasin overturning circulation response described above is also associated with an interbasin heat

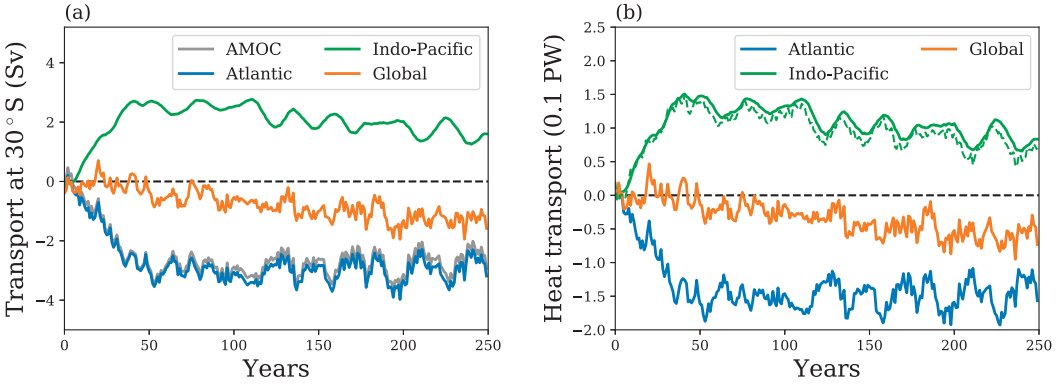

FIG. 4. Anomalies in volume and heat transport following a weakening of AMOC strength in the MITgcm ocean-only simulations. (a) Meridional volume transport anomaly (Sv) in the upper 1 km across 30°S in the Atlantic (blue), Indo-Pacific (green), and the sum of these two basins (orange). The AMOC strength anomaly at 30°S, defined as the maximum value of the overturning circulation streamfunction, is plotted as a gray line. (b) Overturning-driven meridional heat transport anomaly (PW) [Eq. (A4)] across 30°S in the Atlantic (blue), Indo-Pacific (green), and the sum of these two basins (orange). The meridional heat transport anomaly due to all processes in the Indo-Pacific is plotted as a green dashed line for comparison. Unless otherwise noted, time series throughout this study are smoothed using a 5-yr running mean to suppress noise.

transport that effectively redistributes heat from the high-latitude North Atlantic into the Indo-Pacific basins. This transient redistribution occurs via the same mechanism, but with the opposite sense, that transports heat or buoyancy from the low-latitude Pacific to sites of heat loss and NADW formation in the mean state, discussed in Newsom and Thompson (2018). Associated with the AMOC weakening, there is an anomalous overturning-driven southward heat transport out of the Atlantic basin that peaks at ~0.15 PW after about 50 years and then remains roughly constant over the next 200 years (blue line in Fig. 4b). This southward heat transport anomaly leads to a surface cooling and an anomalous surface heat uptake in the high-latitude North Atlantic due to the surface temperature relaxation boundary condition (not shown). The anomalous southward heat transport in the Atlantic basin is largely compensated by a northward overturning-driven heat transport anomaly into the Indo-Pacific basins across 30°S (green solid line in Fig. 4b), which dominates the total meridional heat transport anomaly by all processes combined (green dashed line in Fig. 4b). This heat transport compensation is around 100% during the first 100 years and then slowly decreases to around 70% at the end of the 250-yr simulation. The sum of the meridional heat transport anomalies across 30°S in the Atlantic and Indo-Pacific leaves a smaller residual that represents the net heat transport anomaly into the Southern Ocean. This residual transport slowly intensifies over the duration of the simulation; it is about a third of the magnitude of the Atlantic heat transport anomaly after 250 years (orange line in Fig. 4b).

Advection of a temperature anomaly by the unperturbed flow does not play a significant role in the interbasin heat transport that connects the high-latitude North Atlantic and the Indo-Pacific basins, at least in these simulations (see discussion in 5a). The time scale for an advective change of this nature would be a century or longer, depending on the flow characteristics (cf. Fig. 4b). Instead, the heat transport anomaly is enacted through changes to the circulation strength and structure, which include a deepening of the stratification or density surfaces. This deepening is initiated by a reduction in NADW formation, which converges mass in the upper Atlantic basin, and is then propagated into the Indo-Pacific basins in the forms of coastal and equatorial Kelvin waves (Sun et al. 2020b; Sun and Thompson 2020).

The heat transport convergence into the Indo-Pacific basins by the transient interbasin overturning circulation warms the Indo-Pacific (Fig. 1), but it requires a careful assessment of the temperature changes to isolate this contribution to the total basin-scale warming signal. To do this, we examine the evolution of the vertical temperature distribution, horizontally averaged over the Indo-Pacific basins, in Eulerian depth space (Fig. 5a). The potential temperature field (θ) in the model interior evolves following

$$\frac{\partial \theta}{\partial t} + \nabla_h \cdot (\mathbf{V}_h \theta) + \frac{\partial (w\theta)}{\partial z} = \frac{\partial}{\partial z}\left(\kappa \frac{\partial \theta}{\partial z}\right) + \mathscr{R}, \tag{3}$$

where $\mathbf{V}_h = (u, v)$ is the horizontal velocity vector, the subscript h represents the horizontal direction, and κ is diapycnal diffusivity, which we assume only varies as a function of depth. The first term on the right-hand side represents small-scale diapycnal diffusion while the second term $\mathscr{R}$ represents eddy-induced isopycnal diffusion. Integrating Eq. (3) horizontally over the Indo-Pacific basins and dividing it by the Indo-Pacific basins area (A_{IP}), we obtain the evolution of the basin-averaged temperature profile,

$$\tilde{\theta} = \frac{1}{A_{\mathrm{IP}}} \int\int_{\mathrm{IP}} \theta \, dx \, dy, \tag{4}$$

which is a function of depth and time and is given by

$$\frac{\partial \tilde{\theta}}{\partial t} = \frac{1}{A_{\mathrm{IP}}}\left[\int_{x_w}^{x_e} (v\theta)_{30^\circ\mathrm{S}} \, dx - \int\int_{\mathrm{IP}} \frac{\partial (w\theta)}{\partial z} \, dx \, dy\right] + \frac{\partial}{\partial z}\left(\kappa \frac{\partial \tilde{\theta}}{\partial z}\right) + \mathscr{R}. \tag{5}$$

In the perturbed simulation, changes in both the circulation and the temperature distribution can contribute to the evolution of the temperature anomaly away from the Control simulation, $\tilde{\theta}' = \tilde{\theta}_p - \tilde{\theta}_c$:

$$\frac{\partial \tilde{\theta}'}{\partial t} = \frac{1}{A_{\mathrm{IP}}} \int_{x_w}^{x_e} (v'\theta_c + v_c\theta')_{30^\circ\mathrm{S}} \, dx - \frac{1}{A_{\mathrm{IP}}} \int\int_{\mathrm{IP}} \frac{\partial (w'\theta_c + w_c\theta')}{\partial z} \, dx \, dy + \frac{\partial}{\partial z}\left(\kappa \frac{\partial \tilde{\theta}'}{\partial z}\right) + \mathscr{R}', \tag{6}$$

which is linearized by dropping the nonlinear terms, involving $v'\theta'$ and $w'\theta'$. Here, terms with a subscript c are properties evaluated in the equilibrated Control simulation. Our earlier heat budget analysis suggests that the Indo-Pacific warming is driven by an anomalous northward heat transport across the southern boundary, which is dominated by overturning circulation changes (Figs. 4b and 5b). The contributions to the heat transport anomaly due to advection of temperature anomalies and the nonlinear terms are smaller than the contribution due to overturning circulation changes, as discussed in section 5a. Therefore, we drop the temperature advection tendency terms that arise from temperature changes ($v_c\theta'$ and $w_c\theta'$) in the equation for $\tilde{\theta}'$. We further approximate the temperature field in the Control simulation, θ_c, using the basin-averaged temperature profile, $\tilde{\theta}_c(z)$, since the temperature gradient in the Control simulation is mainly in the vertical direction. This also motivates us to neglect the isopycnal diffusion term and to replace w' with the basin-averaged vertical velocity anomaly, $\tilde{w}'$, which must be in balance with the Eulerian-mean overturning circulation streamfunction anomaly at the southern boundary (ψ'_{S}) (Fig. 5c), that is, $\tilde{w}' = -\psi'_{\mathrm{S}}/A_{\mathrm{IP}}$. With these simplifications, we obtain a vertical advection–diffusion equation for $\tilde{\theta}'$,

$$\frac{\partial \tilde{\theta}'}{\partial t} \approx \frac{1}{A_{\mathrm{IP}}}\left(-\frac{\partial \psi'_{\mathrm{S}}}{\partial z}\tilde{\theta}_c + \frac{\partial \psi'_{\mathrm{S}}\tilde{\theta}_c}{\partial z}\right) + \frac{\partial}{\partial z}\left(\kappa \frac{\partial \tilde{\theta}'}{\partial z}\right) = -\tilde{w}'\frac{\partial \tilde{\theta}_c}{\partial z} + \frac{\partial}{\partial z}\left(\kappa \frac{\partial \tilde{\theta}'}{\partial z}\right). \tag{7}$$

This advection–diffusion relationship is not intended to reproduce the MITgcm simulations but is introduced to illustrate

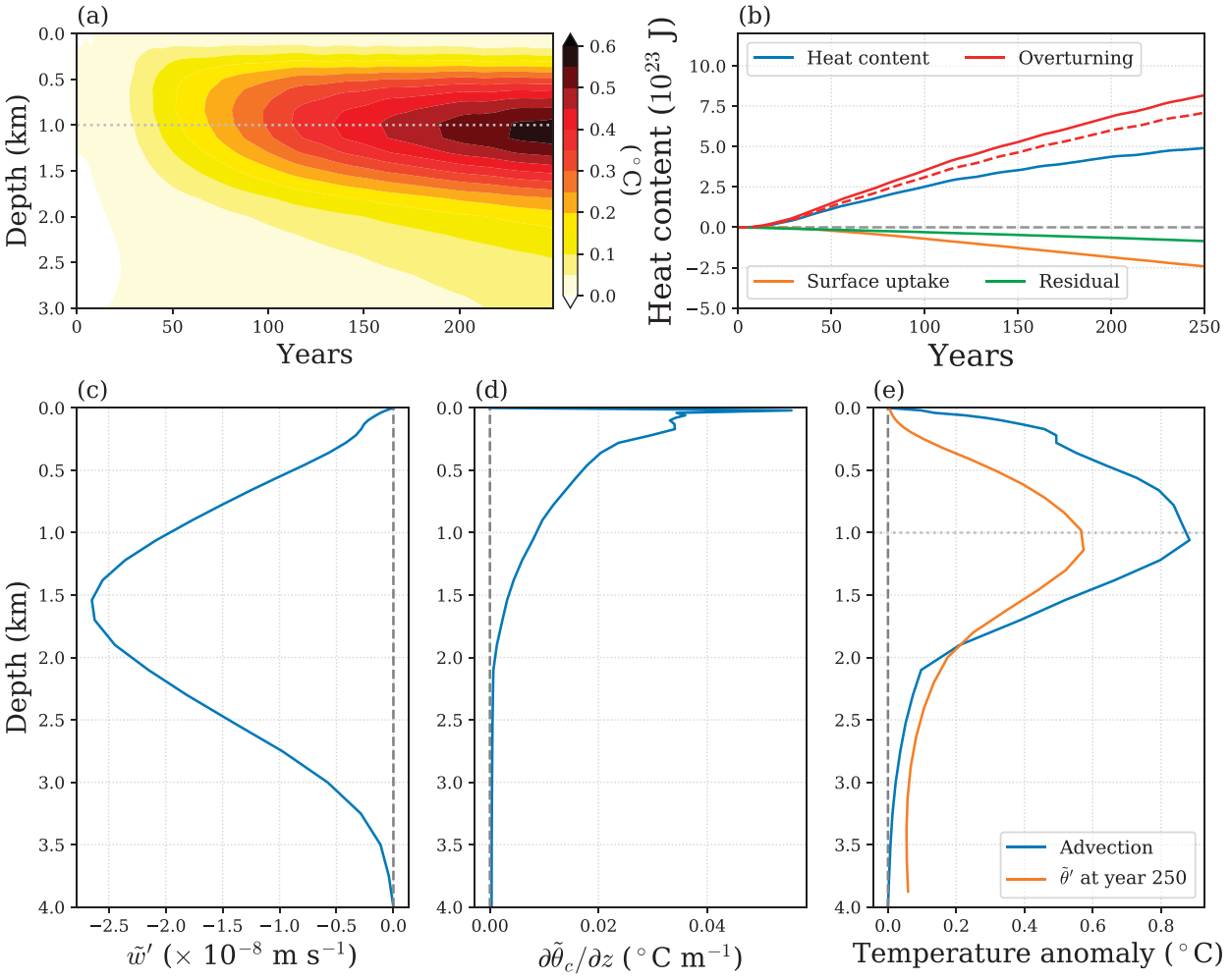

FIG. 5. Subsurface warming and heat budget of the Indo-Pacific basins in the MITgcm ocean-only simulations. (a) Hovmöller diagram of the temperature anomaly ($\tilde{\theta}'$), horizontally averaged over the Indo-Pacific basins, in the perturbed run. (b) Total heat content change (blue) decomposed into anomalous surface heat uptake (orange), heat transport anomalies across the southern boundary by the overturning circulation (red), and the residual (green) [Eq. (2)]. The red dashed line represents the heat content increase due to overturning circulation changes, estimated in the Eulerian depth space [integration of Eq. (1)]. (c) Vertical velocity anomaly [w' in Eq. (7)] in balance with the Indo-Pacific Eulerian-mean overturning circulation changes at 30°S, averaged over the last 50 years. (d) Vertical temperature gradient ($\partial\tilde{\theta}_c/\partial z$) horizontally averaged over the Indo-Pacific basins in the Control simulation. (e) Temperature anomaly in the Indo-Pacific due to vertical advection, integrated over 250 years [Eq. (10); blue], compared to the simulated warming at the end of the 250-yr simulation ($\tilde{\theta}'$; orange). The gray dotted lines in (a) and (e) mark the approximate depth of maximum warming in the perturbed run due to freshwater hosing.

the impact of overturning circulation changes on the basin's temperature evolution. The volume integration of Eq. (7) over the Indo-Pacific, multiplied by $\rho_0 c_p$, is given by

$$\frac{\partial \mathcal{T}'}{\partial t} \approx \rho_0 c_p \int_{-z_{\rm bot}}^{0} \left(\frac{\partial \psi_{\rm S}' \tilde{\theta}_c}{\partial z} - \frac{\partial \psi_{\rm S}'}{\partial z} \tilde{\theta}_c \right) dz + H'_{\rm sfc}$$
$$= \rho_0 c_p \int_{-z_{\rm bot}}^{0} - \frac{\partial \psi_{\rm S}'}{\partial z} \tilde{\theta}_c \, dz + H'_{\rm S}, \tag{8}$$

where

$$\int_{-z_{\rm bot}}^{0} \frac{\partial \psi_{\rm S}' \tilde{\theta}_c}{\partial z} \, dz = \left(\psi_{\rm S}' \tilde{\theta}_c \right) \Big|_{-z_{\rm bot}}^{0} = 0,$$

and the boundary conditions

$$\iint_{\rm IP} \kappa \frac{\partial \tilde{\theta}'}{\partial z} \, dx \, dy = \frac{H'_{\rm sfc}}{\rho_0 c_p} \quad \text{at } z = 0,$$
$$\iint_{\rm IP} \kappa \frac{\partial \tilde{\theta}'}{\partial z} \, dx \, dy = 0 \quad \text{at } z = -z_{\rm bot}, \tag{9}$$

have been used. Thus, heat content changes in the Indo-Pacific basins ($\mathscr{T}'$) have contributions mainly from the heat transport anomaly arising from perturbations in the overturning circulation [red dashed line in Fig. 5b; Eq. (1)] and surface heat uptake H'_{sfc} (orange line in Fig. 5b).

Following a weakened AMOC, the Indo-Pacific develops an overturning circulation anomaly ($\psi'_{\mathrm{S}} > 0$) that opposes the Atlantic changes, associated with an anomalous downwelling ($w' < 0$) and a warming in the Indo-Pacific that peaks at the around 1 km depth ($-w'\partial\tilde{\theta}_c/\partial z > 0$; Figs. 5c–e). To compare the subsurface warming driven by ψ'_{S} with the temperature evolutions in the MITgcm simulations, we integrate the vertical advection term in Eq. (7) in time over 250 years,

$$\tilde{\theta}' \sim -\int_0^{250\mathrm{yr}} w' \frac{\partial \tilde{\theta}_c}{\partial z}\, dt. \tag{10}$$

We find that $\tilde{\theta}'$, derived from (10), qualitatively reproduces the structure of the simulated subsurface warming (Fig. 5e). Critically, the subsurface warming arises from a combination of the structure of overturning circulation anomaly and its correlation with the vertical temperature profile (Figs. 5c,d). The warming has a weaker contribution from diapycnal mixing (differences between the blue and orange lines in Fig. 5e), which actually diffuses the laterally induced subsurface warming vertically and leads to an anomalous surface heat loss (orange line Fig. 5b).

Both the MITgcm simulations and the advection–diffusion model demonstrate that a reduced AMOC would drive a heat transport convergence into the Indo-Pacific across the southern boundary, providing an interbasin pathway for a slow centennial-scale subsurface warming in the Indo-Pacific basins. This subsurface warming is largely due to an adiabatic deepening of the isopycnals, driven by the transient interbasin overturning circulation (see text S1 of the supplemental material). Rather than a downward diffusion of heat following surface warming, here diapycnal mixing results in an upward heat flux as the subsurface temperature anomaly diffuses upward. This upward flux may significantly modify the surface air–sea heat flux (e.g., orange line in Fig. 5b), implying that the transient interbasin overturning circulation may contribute to the pattern of ocean surface warming (Xie et al. 2010) as well as the strength of regional radiative feedback in a changing climate (Armour et al. 2013). A further discussion of the interbasin heat redistribution in the context of a proposed bipolar seesaw mechanism is provided in section 5b.

4. Indo-Pacific warming due to AMOC slowdown in a warming climate

The MITgcm ocean-only simulations indicate that an interbasin heat exchange driven by an AMOC weakening can contribute substantially to the warming of the Indo-Pacific basins. Yet, these ocean-only simulations miss key components of the climate system, including some that may also influence ocean basin heat content. Thus, the robustness of the interbasin heat redistribution is next tested in a more realistic context—a coupled climate simulation under an abrupt CO_2 quadrupling forcing. In the coupled model, the interbasin heat transport, driven by the AMOC weakening, also contributes substantially to a slow subsurface warming of the Indo-Pacific basins once the ocean surface mixed layer equilibrates with the atmosphere.

a. Changes in circulation and heat transport

In response to the abrupt CO_2 quadrupling, there is an initial weakening of the AMOC and a southward transport anomaly in the upper Indo-Pacific basins of roughly 3 Sv that is short-lived, decaying away within the first decade of the simulation (Fig. 6a; negative values represent southward transport). These initial, subdecadal-scale responses occur due to adjustments to a southward shift in the position of the Southern Hemisphere westerly wind following the CO_2 quadrupling (e.g., Rugenstein et al. 2016; Menzel and Merlis 2019). Specifically, this shift produces an easterly wind anomaly near 30°S (not shown) that is accompanied by an anomalous southward Ekman transport, which manifests as a strengthening of the shallow overturning circulation. This upper-ocean circulation change accounts for the southward heat transport anomaly across 30°S during the first decades in both the Atlantic and the Indo-Pacific basins (Fig. 6b). After the initial decadal response, as the circulation adjusts to changes in the surface wind stress curl via the propagation of Rossby waves across the basin, the wind-driven gyre circulation becomes slightly weaker than the preindustrial control state. Subsequently, the gyre does not contribute substantially to changes in the heat transport (see further discussion in text S2 of the supplemental material).

The focus of the remainder of this section is on the centennial-scale overturning circulation changes and its contribution to the heat budget, that is, the evolution that follows the initial transient decadal response. As shown in Sun and Thompson (2020), the AMOC strength at 30°S weakens by around 8 Sv (40%) during the first 100 years in response to the CO_2 quadrupling and then recovers by ~4 Sv in the following 150 years (gray line in Fig. 6a). Similar to the MITgcm simulations in section 3, the Indo-Pacific overturning circulation substantially compensates the AMOC changes (blue and green line in Fig. 6a), leaving the Southern Ocean overturning circulation largely unchanged during this 250-yr simulation (orange line in Fig. 6a).

The rate of surface heat uptake by the ocean also changes dramatically during the 250-yr simulations. During the first 50 years, the Indo-Pacific basin-averaged surface heat flux anomaly decays from around 9 to 0 W m^{-2} (positive indicates surface heat uptake) (Fig. 7a), suggesting an approximate thermal balance between the atmosphere and the ocean surface mixed layer in the Indo-Pacific basins. The Indo-Pacific stands in contrast with the Atlantic Ocean and the Southern Ocean, which have large positive surface heat flux anomalies throughout the 250-yr simulations, related to the upwelling of deep waters. The Atlantic surface heat flux anomaly, which is largely localized in the subpolar North Atlantic (not shown), changes due to the AMOC evolution, increasing from 6 to 8 W m^{-2} as the AMOC weakens and then decreasing to

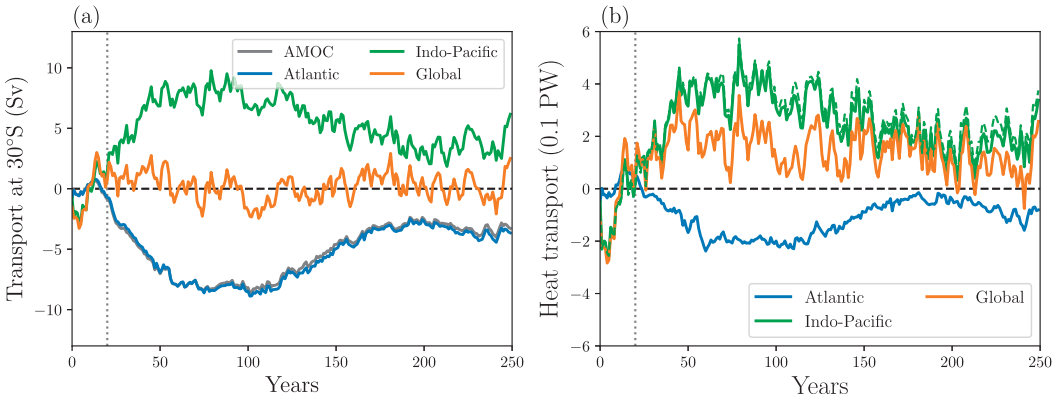

FIG. 6. Time series of the volume and heat transport anomalies in response to CO_2 quadrupling in CCSM4, similar to Fig. 4. (a) Meridional volume transport anomaly (Sv) in the upper 1 km across 30°S in the Atlantic (blue), Indo-Pacific (green), and the sum of these two basins (orange). The AMOC strength anomaly at 30°S is plotted as a gray line. (b) Overturning-driven meridional heat transport anomaly (PW) [Eq. (A4)] across 30°S in the Atlantic (blue), Indo-Pacific (green), and the sum of these two basins (orange). The meridional heat transport anomaly by all processes in the Indo-Pacific is plotted as a green dashed line for comparison. The gray dotted line marks year 20, when the slow subsurface warming in Indo-Pacific begins.

around 4 W m^{-2} at the end of the 250-yr simulation as the AMOC recovers (e.g., Shi et al. 2018; Figs. 6a and 7a). The Southern Ocean surface heat flux anomaly, seemingly independent of the AMOC evolution, slowly decreases from 8 to around 3 W m^{-2} within 250 years. The different surface heat uptake rates between the Atlantic and Indo-Pacific basins, and the Southern Ocean in response to the abrupt CO_2 forcing leads to thermal steric height gradients between these

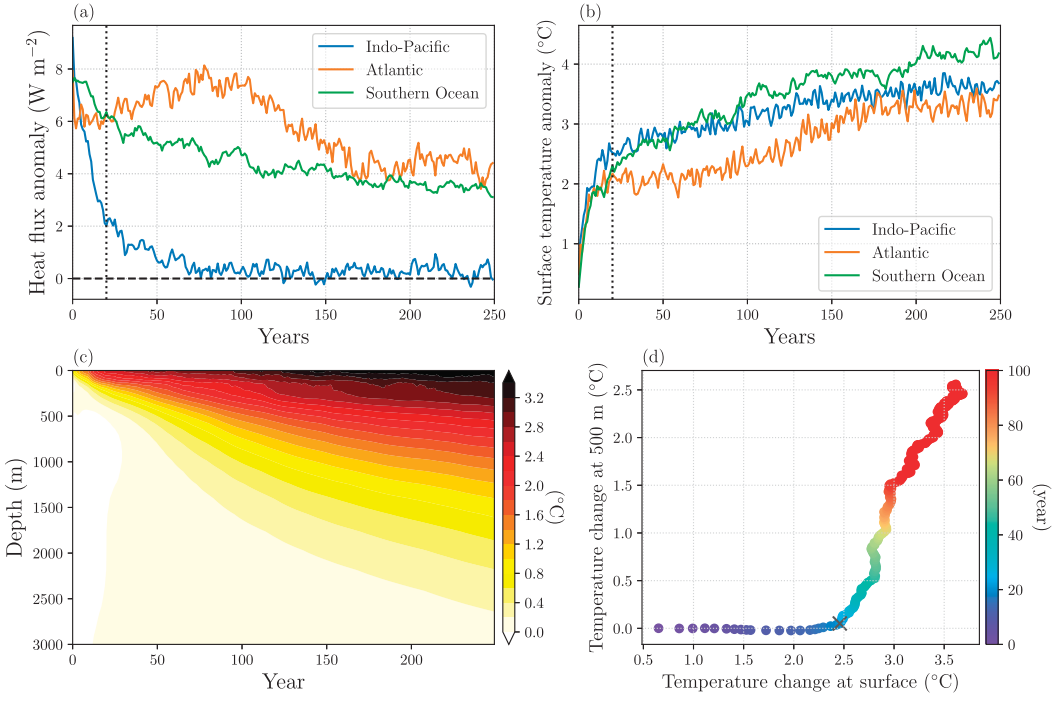

FIG. 7. Warming of the ocean basins after CO_2 quadrupling in CCSM4. (a) Basin-averaged surface heat flux anomaly (W m^{-2}) in the Atlantic (orange), Indo-Pacific (blue), and Southern Ocean (green). (b) Basin-averaged surface temperature anomaly (°C) in the Atlantic (orange), Indo-Pacific (blue), and Southern Ocean (green). (c) Hovmöller diagram of the temperature anomaly ($\tilde{\theta}'$), horizontally averaged in the Indo-Pacific basins. (d) Scatterplot of the temperature anomaly at 500 m vs the temperature anomaly at the surface, horizontally averaged in the Indo-Pacific basins. The color indicates years after CO_2 quadrupling. The black dotted lines in (a) and (b) and the × symbol in (d) indicate year 20, after which the Indo-Pacific temperature evolution is dominated by a subsurface warming.

basins and, thus, necessitates an interbasin heat exchange to remove this gradient (Newsom et al. 2021).

Similar to the ocean-only simulations, as the AMOC weakens, starting 20 years after the CO_2 perturbation, the Atlantic develops a southward heat transport anomaly and the Indo-Pacific develops a northward heat transport anomaly across the southern boundaries (blue and green lines Fig. 6b). However, unlike the ocean-only simulations in which the residual meridional heat transport anomaly into the Southern Ocean is close to zero due to a large cancellation between Indo-Pacific and Atlantic anomalies, in the coupled simulations the magnitude of the Indo-Pacific heat transport anomaly is roughly 2 times as large as the Atlantic heat transport anomaly. This leads to a net northward heat transport anomaly out of the Southern Ocean (orange line in Fig. 6b), which is required to balance the anomalous positive heat uptake in the Southern Ocean throughout the 250-yr simulations (Fig. 7a). Since the volume transport anomalies are of similar magnitude between the Indo-Pacific and the Atlantic, the asymmetry in the meridional heat transport anomaly must be due to the different vertical temperature distribution between these two basins. The vertical temperature gradient is smaller in the Atlantic as compared to the Indo-Pacific because NADW is warmer and saltier than its deep water counterpart in the Indo-Pacific (see details in section 5c). This interbasin difference in temperature and salinity properties is not reproduced in the MITgcm ocean-only runs. Changes in the gyre circulation due to the southward shift of the SH westerlies do not strongly impact the heat transport asymmetry (see text S2 of the supplemental material).

b. *Slow subsurface warming in the Indo-Pacific*

In response to the abrupt CO_2 forcing, the Indo-Pacific warms on two distinct time scales (Figs. 7b,d). The Indo-Pacific basin-averaged surface temperature increases by ~2°C in 20 years. This first stage is the "fast warming," which is mainly confined to the surface mixed layer (Figs. 7c,d). The fast warming is followed by a "slow warming" phase of similar magnitude that occurs over the next ~200 years. In contrast to the fast warming phase, the slow warming is characterized by a warming signal that is larger in the subsurface than at the surface (Fig. 7d). We present the vertical structure of the slow warming in the Indo-Pacific by calculating the temperature anomaly with respect to the temperature profile at year 20, following Long et al. (2014). The temperature evolution shows a subsurface warming pattern with temperatures increasing by more than 1°C down to 1.5 km depth within 250 years (Fig. 8a). In previous studies this slow subsurface warming has been attributed to a diffusive (downward) heat flux that transfers heat from the surface into the deep ocean (Held et al. 2010; Long et al. 2014). However, applying the model's upper-ocean (from the mixed layer base to 1 km) mean diapycnal diffusivity of 2×10^{-5} m^2 s^{-1}, a rough estimate for the time scale τ at which diffusion affects the temperature at a depth $d = 1$ km, $\tau \sim d^2/\kappa$, is around 1500 years. This is substantially longer than the time scale associated with the simulated warming of the deep Indo-Pacific Ocean (Fig. 7c) and suggests the need to identify a different process to account for the deep warming. We suggest that the deeper warming is instead due to the interbasin overturning circulation.

Changes in the subsurface temperature during the slow warming phase peak at around 400 m, much shallower than the overturning circulation responses (Figs. 8c,e). This mainly arises from the sharp decrease in the vertical temperature gradient with depth, although there is an additional contribution from diffusion, which is mainly confined to the upper ocean as discussed below. We estimate the temperature evolution related to the overturning circulation changes by integrating the advection–diffusion equation [Eq. (7)] in time. The integration of the vertical advection term alone [Eq. (10)] approximately reproduces the slow warming at year 250 below 1.5 km (Fig. 8e), suggesting that the deep warming is driven by the interbasin overturning circulation. However, this approach substantially underestimates the simulated warming at shallower depths (Fig. 8e). Part of this underestimation is due to the neglected vertical diffusion. We estimate the temperature changes due to vertical diffusion alone, which was highlighted in Held et al. (2010) as the driver of the deep ocean warming, by solving a diffusion equation [cf. Eq. (7)],

$$\frac{\partial \tilde{\theta}'}{\partial t} = \frac{\partial}{\partial z}\left(\kappa \frac{\partial \tilde{\theta}'}{\partial z}\right), \tag{11}$$

with the boundary conditions as follows:

$$\begin{aligned} \kappa \frac{\partial \tilde{\theta}'}{\partial z} &= F'_{\mathrm{sfc}} \quad \text{at } z = 0, \\ \kappa \frac{\partial \tilde{\theta}'}{\partial z} &= 0 \quad \text{at } z = -z_{\mathrm{bot}}. \end{aligned} \tag{12}$$

Here, $\rho_0 c_p F'_{\mathrm{sfc}} = H'_{\mathrm{sfc}}/A_{\mathrm{IP}}$ is the Indo-Pacific surface heat flux anomaly, given by the blue line in Fig. 7a, and κ is reported by the model and horizontally averaged over the Indo-Pacific basins. Driven by the anomalous surface heat flux due to CO_2 forcing, the temperature changes, from year 20 to year 250, due to vertical diffusion (orange line in Fig. 8e) also peak at the subsurface, with a similar magnitude as the temperature change due to the advection term (blue line in Fig. 8e). However, this diffusive subsurface warming is confined to a shallower depth, mainly in the upper 1 km. Accounting for both vertical advection and diffusion, that is, solving the advection–diffusion equation, Eq. (7), with the boundary conditions (12), we recover a larger subsurface warming that comes closer to reproducing the simulated evolution of the temperature profile (green and red lines in Fig. 8e). The additional underestimated warming in the upper 1 km after accounting for both vertical advection and diffusion, we speculate, is largely due to our calculation of the overturning-driven temperature changes in Eulerian space, as discussed in the heat budget analysis below.

Despite a weak surface heat uptake anomaly after year 50 (Fig. 7a), the Indo-Pacific heat content increases steadily and at approximately the same rate throughout the 250-yr

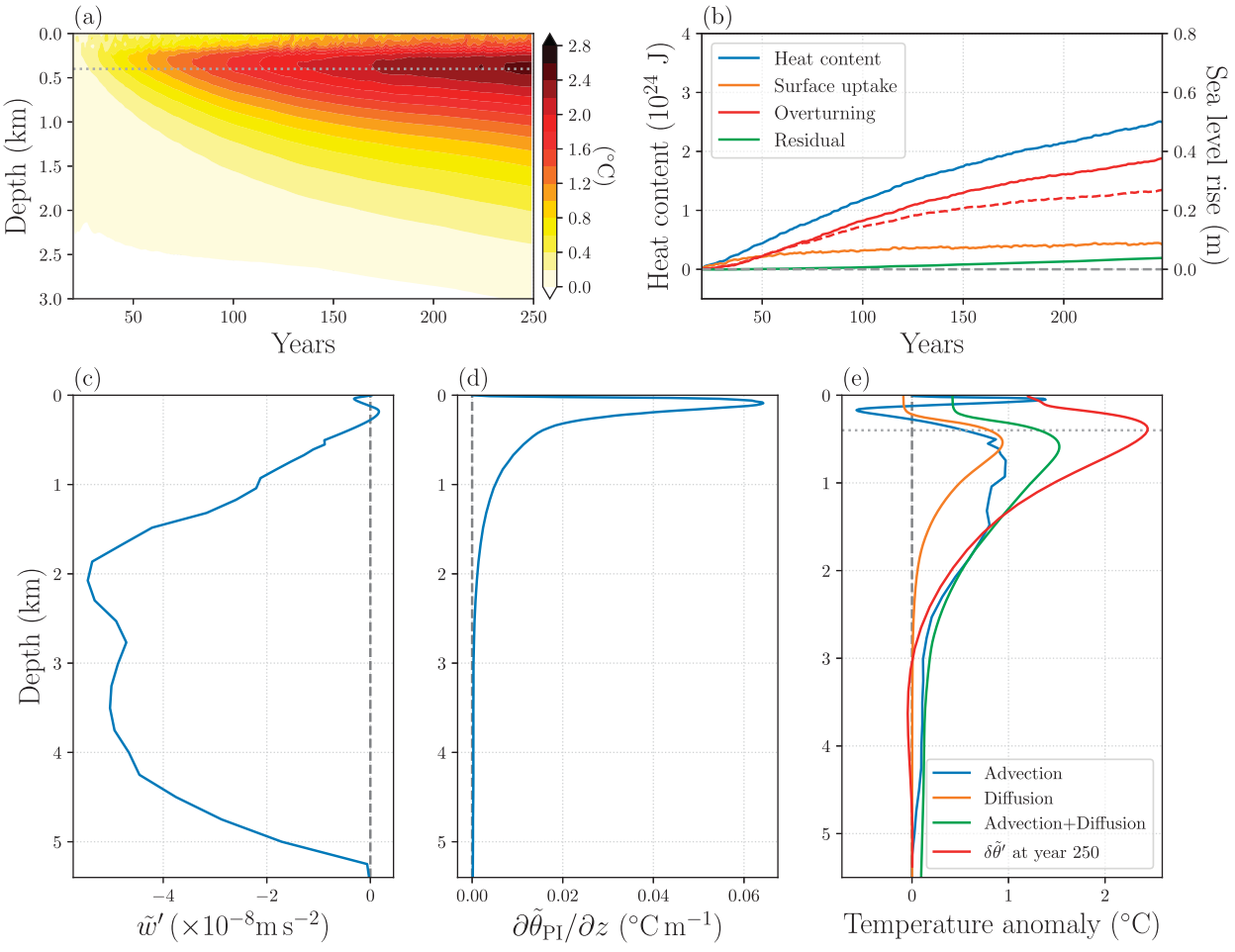

FIG. 8. Subsurface warming and heat budget of the Indo-Pacific basin for the slow warming in CCSM4 (cf. Fig. 5). (a) Hovmöller diagram of the temperature anomaly ($\delta\tilde{\theta}'$; in reference to year 20) in the CCSM4 4xCO_2 experiment, horizontally averaged over the Indo-Pacific basins. (b) Heat content changes (blue) due to anomalous surface heat uptake (orange), heat transport anomalies across the southern boundary by the overturning circulation (red), and the residual (green). The heat content increase driven by changes in the Eulerian-mean overturning circulation is given by the red dashed line. The equivalent sea level rise, calculated using a constant thermal expansion coefficient of 1.5×10^{-4} °C^{-1}, due to heat content increase is labeled on the right ordinate axis. (c) Vertical velocity anomaly in balance with the Indo-Pacific overturning circulation changes at 30°S, averaged over the 250-yr simulation. (d) Vertical temperature gradient horizontally averaged over the Indo-Pacific basin in the PI run. (e) Temperature changes during the slow warming phase, from years 20 to 250, due to overturning-driven vertical advection [Eq. (10); blue], vertical diffusion [Eq. (11); orange], and the combination of both vertical advection and diffusion [Eq. (7); green]. The temperature anomaly at year 250, associated with the slow warming [see (a)], is plotted as a green line for comparison.

simulation (blue line in Fig. 8b). A heat budget analysis shows that roughly 75% of the heat content increase and sea level rise during the slow warming, estimated between year 20 and year 150, is due to the heat transport anomaly across the southern boundary by the overturning circulation (red solid line in Fig. 8b), with the remaining 25% mainly due to surface heat uptake (orange line in Fig. 8b). The heat transport anomaly by the overturning circulation, estimated in the Eulerian space, is smaller than that estimated in isopycnal coordinate (red dashed line vs red solid line in Fig. 8b), likely accounting for the underestimated subsurface warming by the advection–diffusion equation (green and red lines Fig. 8e).

The above analysis highlights interbasin heat redistribution, driven by a weakening of the AMOC, as a major source for the continued heat content changes and sea level rise in the Indo-Pacific basins following a fast surface mixed layer warming (Fig. 8b). This dominance of the interbasin exchange holds even in a coupled climate model where the surface heat uptake is not constrained by imposed surface boundary conditions. This slow warming, peaking at the subsurface, occurs on centennial time scales as volume converges within the upper ocean and is connected to changes in high-latitude processes that modify the ocean overturning circulation (Thompson et al. 2019; Sun and Thompson 2020).

5. Discussion

a. *Passive versus active warming*

The simulations in this study emphasize the role that circulation changes have on ocean heat transport and the convergence of heat into certain regions of the ocean, a mechanism that has been referred to as "active warming." However, changes to the ocean's temperature distribution can also contribute to heat transport anomalies, even in the absence of a change in the ocean circulation, a mechanism referred to as "passive warming." In the ocean-only simulations, despite a relaxation boundary condition that can change the net surface heat flux, modifications to the vertical temperature profile due to the subsurface warming do not substantially change the vertical temperature gradient from the control state (Figs. 5a,d), and thus, the heat transport anomaly is predominantly due to the overturning circulation changes. However, in the CCSM4 experiments, due to the larger atmospheric perturbation, the ocean's temperature fields evolve due to radiative forcing and can feedback on the ocean heat transport. Here we compare the contributions to the meridional heat transport across 30°S due to circulation changes and temperature changes in the Atlantic and Indo-Pacific basins in the CCSM4 4xCO_2 experiment.

The meridional ocean heat transport anomaly across 30°S in the 4xCO_2 experiment, relative to the preindustrial (PI) run and including contributions from both the gyre circulations as well as the deeper overturning circulation, can be decomposed into three components: changes in circulation, changes in temperature, and changes in both (e.g., Hu et al. 2020). This can be written as

$$H' = \rho_0 c_p \int_{-z_{\text{bot}}}^{0} \int_{x_w}^{x_e} \left(v'\theta_{\text{PI}} + v_{\text{PI}}\theta' + v'\theta'\right) dx\, dz, \qquad (13)$$

where primes denote anomalies from the PI run. In both the Atlantic and Indo-Pacific basins, the second and third terms are small and of opposite sign. The reason for the leading-order cancellation between these two terms is not immediately obvious. However, this cancellation implies that the heat transport anomaly across 30°S is dominated by circulation changes (Figs. 9a,b), such that the dominant contribution to interbasin heat exchange in the CCSM4 4xCO_2 experiment is linked to overturning circulation changes caused by the AMOC weakening (Figs. 6b and 9).

Although the results of this study highlight the role of active warming in interbasin heat exchange, passive warming could be important for the Indo-Pacific heat content changes on certain time scales. Recently, Bronselaer and Zanna (2020) suggested that the projected pattern of heat content changes during the twenty-first century is dominated by passive ocean heat uptake due to increasing atmospheric CO_2 radiative forcing. This passive warming process appears to manifest in the CCSM4 4xCO_2 experiment mainly during the fast warming stage, when the Indo-Pacific heat content changes are mainly due to local surface heat uptake (Fig. 7). However, beyond the twenty-first century when atmospheric CO_2 reaches equilibrium, surface ocean heat uptake mainly occurs in the high-latitude North Atlantic and Southern Ocean, and our results suggest that the Indo-Pacific warming will be predominately due to heat redistribution by the interbasin overturning circulation.

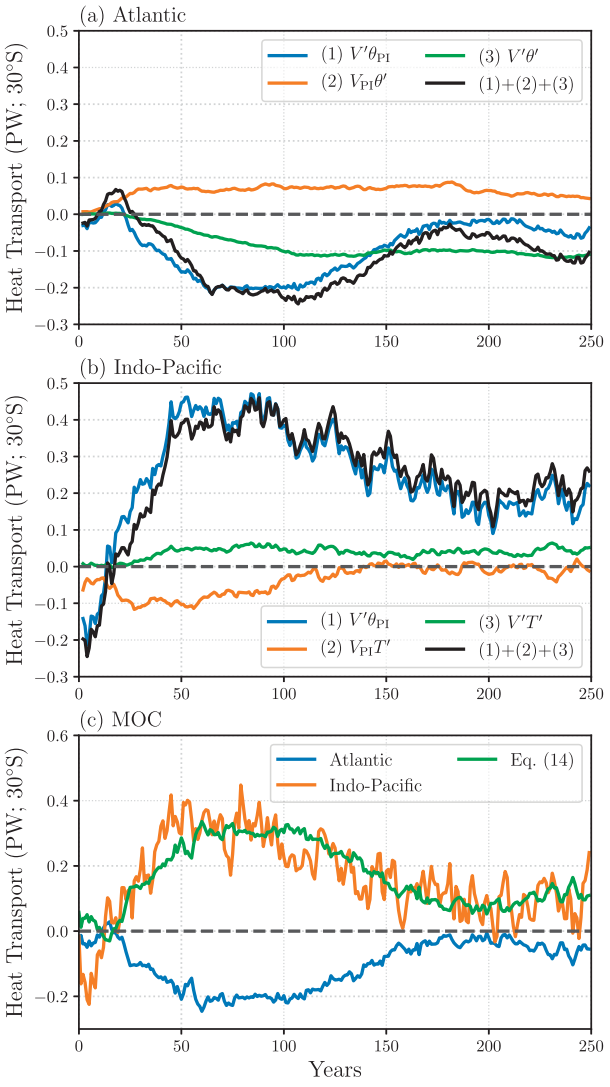

FIG. 9. Heat transport anomaly across 30°S in the CCSM4 abrupt 4xCO_2 experiment in comparison to the preindustrial Control simulation. (a) Heat transport anomaly across 30°S in the Atlantic (black) due to changes in the circulation (blue), changes in temperature (orange), and changes in both (green) [Eq. (13)]. (b) Heat transport anomaly across 30°S in the Indo-Pacific (black) due to changes in the circulation (blue), changes in temperature (orange), and changes in both (green). (c) Heat transport anomaly driven by the Eulerian-mean overturning circulation anomaly [Eq. (1)] in the Atlantic (blue) and Indo-Pacific (orange). The green line represents the heat transport calculated using the Atlantic overturning circulation anomaly applied to the Indo-Pacific temperature profile; the sign of this curve is reversed to more easily compare it with the orange line [opposite sign of Eq. (14); see section 5c for details].

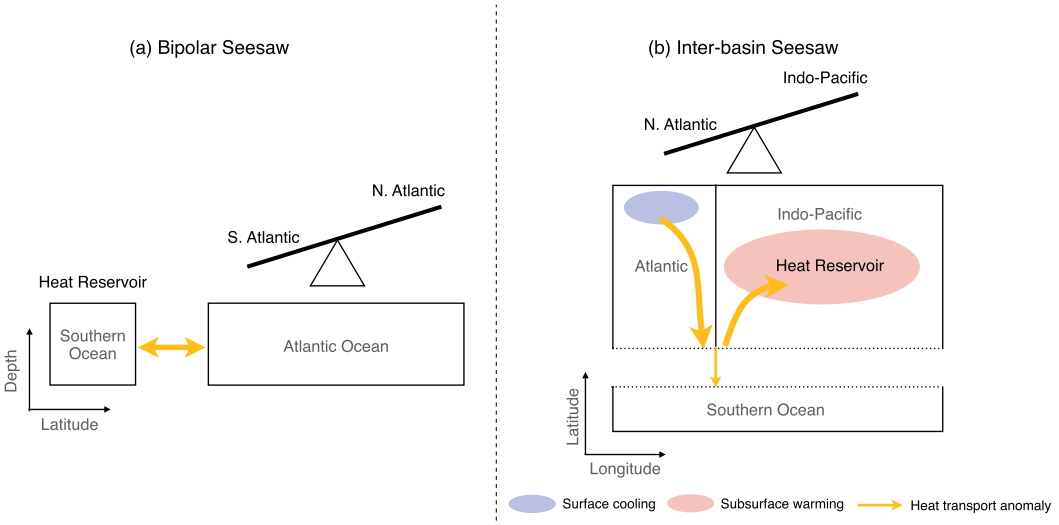

FIG. 10. Schematics of the (a) bipolar seesaw and (b) interbasin seesaw mechanisms. The bipolar seesaw schematic is adapted from Stocker and Johnsen (2003, their Fig. 2), with the double arrow representing heat exchange between the Southern Ocean and South Atlantic due to diffusive processes. In (b), the orange arrows represent the heat transport anomaly following a weakened AMOC, with the magnitude represented by the width of the arrow. The anomalous heat transport into the Southern Ocean is the residual between the Atlantic (southward) and the Indo-Pacific (northward) heat transport anomalies, and it is weaker than the heat transport anomalies in either of the two northern basins. This revised view of centennial-scale overturning adjustment suggests that the Indo-Pacific is the key heat reservoir associated with Dansgaard–Oeschger events during the last glacial period (cf. Stocker and Johnsen 2003; Pedro et al. 2018).

b. *Interbasin seesaw versus bipolar seesaw*

This study has, to this point, largely focused on the implications of Indo-Pacific warming due to future climate change. However, rearrangement of the AMOC and the associated changes in meridional heat transport have also been key features of abrupt climate change events throughout Earth's history. Of particular relevance is the thermal bipolar seesaw, used to describe a change in heat content of the North Atlantic and the Southern Ocean on multicentennial to millennial time scales associated with DO events (Crowley 1992; Stocker and Johnsen 2003). High-latitude forcing, such as Heinrich events, are believed to interrupt NADW formation, after which the AMOC weakens and a southward heat transport anomaly emerges in the Atlantic basin. This southward heat transport anomaly has been postulated as the reason for anticorrelated temperature changes between Greenland and Antarctica during DO events (Crowley 1992): during periods when Greenland warms, Antarctica cools, and vice versa. The more gradual trends in Antarctic temperature as compared to the abrupt Northern Hemisphere changes are explained in Stocker and Johnsen (2003) by assuming that the Southern Ocean acts as a heat reservoir for the southward heat transport (Fig. 10a). More recently, Buizert et al. (2015) used high-accumulation ice cores to show that changes in Northern and Southern Hemispheres temperature were not synchronous, but rather Northern Hemisphere changes lead Southern Hemisphere changes by roughly 200 years. This study provides strong evidence that interhemispheric heat redistribution is carried out by the ocean, rather than atmospheric processes, and furthermore, that this characteristic lag time scale is independent of the background climate state. However, this study did not offer a mechanistic description of the processes that give rise to the 200-yr time scale, although Thompson et al. (2019) suggest that it could be related to the time needed to adjust the stratification and therefore the ventilation of deep waters in the Southern Ocean.

Here we suggest two important updates to the bipolar seesaw theory. First, over a series of studies (Sun et al. 2020b; Sun and Thompson 2020), it has been shown that the initial response to a transition in the AMOC takes place principally in the Indo-Pacific basins, not in the Southern Ocean. This is true for changes in both circulation and heat transport. Second, we suggest an interbasin seesaw, in which the Indo-Pacific, rather than the Southern Ocean, acts as the heat reservoir for the AMOC-driven heat transport changes (Fig. 10b). For instance, when the AMOC weakens during an abrupt Northern Hemisphere cooling event, the southward heat transport anomaly in the Atlantic was likely substantially compensated by a northward heat transport anomaly into the Indo-Pacific basins, driven by the transient interbasin overturning circulation (Fig. 1). This interbasin heat redistribution leads to a cooling in the high-latitude North Atlantic and a subsurface warming in the Indo-Pacific on centennial time scales, that is, an interbasin seesaw. The subsurface warming in the Pacific weakens the upper ocean density stratification and may have additionally contributed to enhanced ventilation in the high-latitude North Pacific during Heinrich events (Walczak et al. 2020).

This transfer of heat into the Indo-Pacific is important for two reasons. First, the Indo-Pacific, at 30°S, dominates the zonal extent of the ocean and for this reason, has a stronger impact on the stratification of and transport into the Southern Ocean—essentially, the Indo-Pacific basins provide the northern boundary condition for the depths of the isopycnals that span the ACC (Nikurashin and Vallis 2012; Thompson et al. 2016; Sun et al. 2018). The anomalous subsurface warming of the Indo-Pacific proceeds changes in the Southern Ocean (Fig. 4a) and provides an efficient pathway for the increased, subsurface heat content in the Indo-Pacific to be transported into the Southern Ocean. Second, the adjustment of the Indo-Pacific basins to changes in the surface forcing that perturbs the AMOC happens over a period of multiple decades to a few centuries. The heat transport anomaly into the Southern Ocean, which arises from a residual between the Atlantic and the Indo-Pacific heat transport anomalies, only slowly increases in magnitude as the Southern Ocean overturning circulation responds on multicentennial time scales (orange lines in Fig. 4). Thus, an interbasin seesaw between the Atlantic and Indo-Pacific helps to explain the more gradual changes in Antarctic temperature paleo-records as compared to the abrupt changes in the high-latitude North Atlantic during the DO events. The 200-yr lag of SH temperature responses in the interhemispheric phase changes is also consistent with the dynamical processes that enable the interbasin exchange, although further studies are needed to confirm the relative importance of this mechanism in the presence of other forcing changes, such as a perturbation to the strength or position of SH westerlies.

The transient compensation in meridional heat transport between the Atlantic and Indo-Pacific basins in response to an AMOC weakening has been reported in previous studies (e.g., Pedro et al. 2018), and is implicitly included in the conceptual model studies by Thompson et al. (2019), but the mechanisms that give rise to this compensation were not explored. Here we connect the interbasin heat transport between the Atlantic and Indo-Pacific basins to a transient interbasin overturning circulation, following AMOC changes.

c. *Southern Ocean's role in the interbasin heat transport*

There remain outstanding questions regarding the Southern Ocean's role in the interbasin heat transport. For instance, the CCSM4 coupled simulation shows that the magnitude of the heat transport response is larger in the Indo-Pacific (H'_{IP}) as compared to the Atlantic (H'_{ATL}), associated with the transient interbasin overturning circulation, that is, $H'_{\mathrm{SO}} = H'_{\mathrm{ATL}} + H'_{\mathrm{IP}} > 0$ (Fig. 6). This behavior differs from the ocean-only simulations in which $H'_{\mathrm{SO}} \leq 0$ (Fig. 4). The interbasin asymmetry in heat transport in the CCSM4 coupled simulation arises from differences in the vertical temperature gradients between the Atlantic and Indo-Pacific basins. This difference in temperature structure is consistent with observations but not simulated in the MITgcm ocean-only runs. To support this, we calculate the hypothetical overturning-driven heat transport anomaly in the Atlantic basin but imposing a temperature profile that is identical to the Indo-Pacific (θ_{IP}), that is,

$$H'_{\mathrm{ATL}} = -\int_{-z_{\mathrm{bot}}}^{0} \frac{\partial \psi'_{\mathrm{ATL}}}{\partial z}\theta_{\mathrm{IP}}\, dz.$$

Indeed, using the same temperature profile in the Indo-Pacific from the PI control run, the heat transport driven by the Eulerian-mean Atlantic overturning circulation (green line in Fig. 9c; reversed in sign for comparison) is approximately the same as the Indo-Pacific (orange line in Fig. 9c). Crucially, a positive (northward) value for H'_{SO} is consistent with an anomalous surface heat uptake that occurs in the Southern Ocean in CCSM4 after the CO_2 quadrupling (Fig. 7). Yet, it is not obvious whether the heat transport anomaly into the Southern Ocean should be positive or negative in the case of a reduction in AMOC strength but no substantial change in the Southern Ocean surface forcing.

6. Summary

Changes in Earth's climate are often associated with a reorganization of the global ocean overturning circulation. Recently, Sun et al. (2020b) showed that there is a transient overturning compensation between the Atlantic and Indo-Pacific basins, following a perturbation in the AMOC. As the AMOC weakens, the Indo-Pacific develops an opposing overturning circulation anomaly, characterized by an anomalous northward surface transport. In this study, we show that this transient interbasin overturning circulation can effectively redistribute heat between the Atlantic and the Indo-Pacific basins, leading to a slow centennial subsurface warming in the Indo-Pacific. This process makes the dominant contribution to changes in ocean heat content in these basins, even in cases where atmospheric warming leads to increased surface heat uptake. We postulate that there is an interbasin seesaw associated with the transient interbasin overturning circulation that also helps to explain why Antarctic temperature records during the last glacial period generally show more gradual changes than the abrupt transitions recorded in the Northern Hemisphere.

By examining an abrupt CO_2 quadrupling experiment in a coupled climate model, which presents a fast decadal surface warming and a slow centennial subsurface warming, we show that the interbasin heat redistribution, driven by a weakening of the AMOC, contributes substantially to the slow subsurface warming and sea level rise in the Indo-Pacific in response to CO_2 forcing (Long et al. 2020). This interbasin pathway for the Indo-Pacific warming, which hinges on adiabatic processes, is separate from the diapycnal processes emphasized in previous studies that occur over millennial time scales due to the downward diffusion of heat into the deep ocean (e.g., Held et al. 2010). The subsurface warming driven by the transient interbasin overturning circulation gives rise to an interior heat anomaly in the ocean that can, over time, diffuse upward and potentially contribute to the pattern of ocean surface warming (Xie et al. 2010), influence regional air–sea heat

fluxes and atmospheric circulation (Kang et al. 2020; Molina et al. 2022), and modulate regional radiative feedback (Armour et al. 2013).

Acknowledgments. Without implying their endorsement, we thank Emily Newsom, Laure Zanna, Spencer Jones, and Dave Bonan for helpful discussions. We are also grateful for constructive comments from Christopher Wolfe and two anonymous reviewers that helped to improve this manuscript. SS and AFT were supported by NSF Award OCE-1756956 and the David and Lucille Packard Foundation. SL acknowledges support from the National Natural Science Foundation of China (42076208 and 41706026). The computations presented here were conducted in the Resnick High Performance Center, a facility supported by Resnick Sustainability Institute at the California Institute of Technology.

Data availability statement. The CCSM4 model output was downloaded from the Climate Data Gateway at NCAR (https://www.earthsystemgrid.org). The code for reproducing the MITgcm ocean-only simulations is provided at the online open access repository, figshare (https://doi.org/10.6084/m9.figshare.16308111).

APPENDIX

Definition of the Overturning Circulation Streamfunction and Heat Transport

The meridional overturning circulation streamfunction in a basin is calculated in σ_2 (potential density referenced to 2000 dbar) coordinate as

$$\Psi(y,\sigma_2)=\frac{1}{t_2-t_1}\int_{t_1}^{t_2}\int_{x_w}^{x_e}\int_{-z_{\rm bot}}^{0}\upsilon_r(x,y,z,t)\times\mathscr{H}\left[\sigma_2-\sigma_2'(x,y,z,t)\right]dzdxdt, \tag{A1}$$

where $\upsilon_r=\upsilon_{\rm Eulerian}+\upsilon_{\rm eddy}$ is the total meridional velocity that includes both the Eulerian-mean flow ($\upsilon_{\rm Eulerian}$) and eddy bolus contribution due to parameterized eddies ($\upsilon_{\rm eddy}$), σ_2' is the potential density field calculated by the model, t_1 and t_2 define the averaging period, and $\mathscr{H}(\sigma_2-\sigma_2')$ is the Heaviside step function of $\sigma_2-\sigma_2'$ such that $\psi(y,\sigma_2)$ represents the northward volume transport above the isopycnal denoted by σ_2.

For presentation purpose, we map the overturning circulation streamfunction Ψ to depth coordinates using the zonal- and time-averaged depth of each isopycnal (Fig. 3)

$$\phi\left[y,\bar{\zeta}(y,\sigma_2)\right]=\Psi(y,\sigma_2), \tag{A2}$$

where $\bar{\zeta}(y,\sigma_2)$ is the zonal and time mean of the isopycnal depth ζ (Nurser and Lee 2004).

In this study, we also use the Eulerian-mean overturning circulation,

$$\psi(y,z)=\frac{1}{t_2-t_1}\int_{t_1}^{t_2}\int_{x_w}^{x_e}\int_{z}^{0}\upsilon_{\rm Eulerian}(x,y,z',t)dz'\,dx\,dt. \tag{A3}$$

As compared to the isopycnal overturning circulation, the Eulerian-mean overturning circulation misses the eddy bolus contribution ($\upsilon_{\rm bolus}$), as well as the contribution due to standing eddies (Viebahn and Eden 2012). The meridional heat transport associated with the isopycnal overturning circulation is calculated as

$$H_{\rm OT}(y)=\rho_0 c_p\int_{\sigma_{\rm min}}^{\sigma_{\rm max}}\frac{\partial\Psi(y,\sigma_2)}{\partial\sigma_2}\hat{\theta}(y,\sigma_2)d\sigma_2. \tag{A4}$$

Here $\hat{\theta}$ is the thickness-averaged temperature (Young 2012), defined as

$$\hat{\theta}(y,\sigma_2)=\frac{\int_{t_1}^{t_2}\int_{x_w}^{x_e}\theta(x,y,\zeta,t)\gamma(x,y,\sigma_2,t)dx\,dt}{\int_{t_1}^{t_2}\int_{x_w}^{x_e}\gamma(x,y,\sigma_2,t)dx\,dt}, \tag{A5}$$

where ζ is the depth of isopycnal σ_2 and $\gamma=\partial\zeta/\partial\sigma_2$ is the isopycnal thickness.

REFERENCES

Armour, K. C., C. M. Bitz, and G. H. Roe, 2013: Time-varying climate sensitivity from regional feedbacks. *J. Climate,* **26**, 4518–4534, https://doi.org/10.1175/JCLI-D-12-00544.1.

Ballarotta, M., S. Drijfhout, T. Kuhlbrodt, and K. Döös, 2013: The residual circulation of the Southern Ocean: Which spatio-temporal scales are needed? *Ocean Modell.,* **64**, 46–55, https://doi.org/10.1016/j.ocemod.2013.01.005.

Barker, S., P. Diz, M. J. Vautravers, J. Pike, G. Knorr, I. R. Hall, and W. S. Broecker, 2009: Interhemispheric Atlantic seesaw response during the last deglaciation. *Nature,* **457**, 1097–1102, https://doi.org/10.1038/nature07770.

Blunier, T., and E. J. Brook, 2001: Timing of millennial-scale climate change in Antarctica and Greenland during the last glacial period. *Science,* **291**, 109–112, https://doi.org/10.1126/science.291.5501.109.

Broecker, W. S., D. M. Peteet, and D. Rind, 1985: Does the ocean–atmosphere system have more than one stable mode of operation? *Nature,* **315**, 21–26, https://doi.org/10.1038/315021a0.

Bronselaer, B., and L. Zanna, 2020: Heat and carbon coupling reveals ocean warming due to circulation changes. *Nature,* **584**, 227–233, https://doi.org/10.1038/s41586-020-2573-5.

Bryan, K., and L. Lewis, 1979: A water mass model of the world ocean. *J. Geophys. Res.,* **84**, 2503–2517, https://doi.org/10.1029/JC084iC05p02503.

Buizert, C., and Coauthors, 2015: Precise interpolar phasing of abrupt climate change during the last ice age. *Nature,* **520**, 661–665, https://doi.org/10.1038/nature14401.

Cessi, P., K. Bryan, and R. Zhang, 2004: Global seiching of thermocline waters between the Atlantic and the Indian-Pacific Ocean basins. *Geophys. Res. Lett.,* **31**, L04302, https://doi.org/10.1029/2003GL019091.

Cheng, W., J. C. Chiang, and D. Zhang, 2013: Atlantic meridional overturning circulation (AMOC) in CMIP5 models: RCP and historical simulations. *J. Climate,* **26**, 7187–7197, https://doi.org/10.1175/JCLI-D-12-00496.1.

Crowley, T. J., 1992: North Atlantic deep water cools the Southern Hemisphere. *Paleoceanography,* **7**, 489–497, https://doi.org/10.1029/92PA01058.

Dansgaard, W., and Coauthors, 1993: Evidence for general instability of past climate from a 250-kyr ice-core record. *Nature,* **364**, 218–220, https://doi.org/10.1038/364218a0.

Forget, G., J.-M. Campin, P. Heimbach, C. Hill, R. Ponte, and C. Wunsch, 2015: ECCO version 4: An integrated framework for non-linear inverse modeling and global ocean state estimation. *Geosci. Model Dev.,* **8**, 3071–3104, https://doi.org/10.5194/gmd-8-3071-2015.

Garuba, O. A., and B. A. Klinger, 2016: Ocean heat uptake and interbasin transport of the passive and redistributive components of surface heating. *J. Climate,* **29**, 7507–7527, https://doi.org/10.1175/JCLI-D-16-0138.1.

Gent, P. R., and Coauthors, 2011: The Community Climate System Model version 4. *J. Climate,* **24**, 4973–4991, https://doi.org/10.1175/2011JCLI4083.1.

Gordon, A. L., 1986: Interocean exchange of thermocline water. *J. Geophys. Res.,* **91**, 5037–5046, https://doi.org/10.1029/JC091iC04p05037.

Gregory, J. M., 2000: Vertical heat transports in the ocean and their effect on time-dependent climate change. *Climate Dyn.,* **16**, 501–515, https://doi.org/10.1007/s003820000059.

Griffies, S. M., and Coauthors, 2009: Coordinated Ocean-ice Reference Experiments (COREs). *Ocean Modell.,* **26** (1–2), 1–46, https://doi.org/10.1016/j.ocemod.2008.08.007.

Haney, R. L., 1971: Surface thermal boundary condition for ocean circulation models. *J. Phys. Oceanogr.,* **1**, 241–248, https://doi.org/10.1175/1520-0485(1971)001<0241:STBCFO>2.0.CO;2.

Held, I. M., M. Winton, K. Takahashi, T. Delworth, F. Zeng, and G. K. Vallis, 2010: Probing the fast and slow components of global warming by returning abruptly to preindustrial forcing. *J. Climate,* **23**, 2418–2427, https://doi.org/10.1175/2009JCLI3466.1.

Hu, S., S.-P. Xie, and W. Liu, 2020: Global pattern formation of net ocean surface heat flux response to greenhouse warming. *J. Climate,* **33**, 7503–7522, https://doi.org/10.1175/JCLI-D-19-0642.1.

Huang, R. X., M. A. Cane, N. Naik, and P. Goodman, 2000: Global adjustment of the thermocline in response to deepwater formation. *Geophys. Res. Lett.,* **27**, 759–762, https://doi.org/10.1029/1999GL002365.

Jackett, D. R., and T. J. Mcdougall, 1995: Minimal adjustment of hydrographic profiles to achieve static stability. *J. Atmos. Oceanic Technol.,* **12**, 381–389, https://doi.org/10.1175/1520-0426(1995)012<0381:MAOHPT>2.0.CO;2.

Jansen, M. F., L.-P. Nadeau, and T. M. Merlis, 2018: Transient versus equilibrium response of the ocean's overturning circulation to warming. *J. Climate,* **31**, 5147–5163, https://doi.org/10.1175/JCLI-D-17-0797.1.

Johnson, H. L., and D. P. Marshall, 2004: Global teleconnections of meridional overturning circulation anomalies. *J. Phys. Oceanogr.,* **34**, 1702–1722, https://doi.org/10.1175/1520-0485(2004)034<1702:GTOMOC>2.0.CO;2.

Kang, S. M., S.-P. Xie, Y. Shin, H. Kim, Y.-T. Hwang, M. F. Stuecker, B. Xiang, and M. Hawcroft, 2020: Walker circulation response to extratropical radiative forcing. *Sci. Adv.,* **6**, eabd3021, https://doi.org/10.1126/sciadv.abd3021.

Liu, W., A. V. Fedorov, S.-P. Xie, and S. Hu, 2020: Climate impacts of a weakened Atlantic meridional overturning circulation in a warming climate. *Sci. Adv.,* **6**, eaaz4876, https://doi.org/10.1126/sciadv.aaz4876.

Liu, Z., and Coauthors, 2009: Transient simulation of last deglaciation with a new mechanism for Bølling-Allerød warming. *Science,* **325**, 310–314, https://doi.org/10.1126/science.1171041.

Long, S.-M., S.-P. Xie, X.-T. Zheng, and Q. Liu, 2014: Fast and slow responses to global warming: Sea surface temperature and precipitation patterns. *J. Climate,* **27**, 285–299, https://doi.org/10.1175/JCLI-D-13-00297.1.

——, ——, Y. Du, Q. Liu, X.-T. Zheng, G. Huang, K.-M. Hu, and J. Ying, 2020: Effects of ocean slow response under low warming targets. *J. Climate,* **33**, 477–496, https://doi.org/10.1175/JCLI-D-19-0213.1.

Markle, B. R., and Coauthors, 2017: Global atmospheric teleconnections during Dansgaard–Oeschger events. *Nat. Geosci.,* **10**, 36–40, https://doi.org/10.1038/ngeo2848.

Marshall, J., and K. Speer, 2012: Closure of the meridional overturning circulation through Southern Ocean upwelling. *Nat. Geosci.,* **5**, 171–180, https://doi.org/10.1038/ngeo1391.

——, A. Adcroft, C. Hill, L. Perelman, and C. Heisey, 1997: A finite-volume, incompressible Navier Stokes model for studies of the ocean on parallel computers. *J. Geophys. Res.,* **102**, 5753–5766, https://doi.org/10.1029/96JC02775.

Menary, M. B., and R. A. Wood, 2018: An anatomy of the projected North Atlantic warming hole in CMIP5 models. *Climate Dyn.,* **50**, 3063–3080, https://doi.org/10.1007/s00382-017-3793-8.

Menzel, M. E., and T. M. Merlis, 2019: Connecting direct effects of CO_2 radiative forcing to ocean heat uptake and circulation. *J. Adv. Model. Earth Syst.,* **11**, 2163–2176, https://doi.org/10.1029/2018MS001544.

Molina, M. J., A. Hu, and G. A. Meehl, 2022: Response of global SSTs and ENSO to the Atlantic and Pacific meridional overturning circulations. *J. Climate,* **35**, 49–72, https://doi.org/10.1175/JCLI-D-21-0172.1.

Newsom, E. R., and A. F. Thompson, 2018: Reassessing the role of the Indo-Pacific in the ocean's global overturning circulation. *Geophys. Res. Lett.,* **45**, 12 422–12 431, https://doi.org/10.1029/2018GL080350.

——, ——, J. F. Adkins, and E. D. Galbraith, 2021: A hemispheric asymmetry in poleward ocean heat transport across climates: Implications for overturning and polar warming. *Earth Plan. Sci. Lett.,* **568**, 117033, https://doi.org/10.1016/j.epsl.2021.117033.

Nikurashin, M., and G. Vallis, 2012: A theory of the interhemispheric meridional overturning circulation and associated stratification. *J. Phys. Oceanogr.,* **42**, 1652–1667, https://doi.org/10.1175/JPO-D-11-0189.1.

Nurser, A. G., and M.-M. Lee, 2004: Isopycnal averaging at constant height. Part I: The formulation and a case study. *J. Phys. Oceanogr.,* **34**, 2721–2739, https://doi.org/10.1175/JPO2649.1.

Pedro, J. B., M. Jochum, C. Buizert, F. He, S. Barker, and S. O. Rasmussen, 2018: Beyond the bipolar seesaw: Toward a process understanding of interhemispheric coupling. *Quat. Sci. Rev.,* **192**, 27–46, https://doi.org/10.1016/j.quascirev.2018.05.005.

Purkey, S. G., and G. C. Johnson, 2013: Antarctic bottom water warming and freshening: Contributions to sea level rise, ocean freshwater budgets, and global heat gain. *J. Climate,* **26**, 6105–6122, https://doi.org/10.1175/JCLI-D-12-00834.1.

Redi, M. H., 1982: Oceanic isopycnal mixing by coordinate rotation. *J. Phys. Oceanogr.,* **12**, 1154–1158, https://doi.org/10.1175/1520-0485(1982)012<1154:OIMBCR>2.0.CO;2.

Rugenstein, M. A., J. M. Gregory, N. Schaller, J. Sedláček, and R. Knutti, 2016: Multiannual ocean–atmosphere adjustments to radiative forcing. *J. Climate,* **29**, 5643–5659, https://doi.org/10.1175/JCLI-D-16-0312.1.

Sen Gupta, A., S. McGregor, E. Van Sebille, A. Ganachaud, J. N. Brown, and A. Santoso, 2016: Future changes to the

Indonesian Throughflow and Pacific circulation: The differing role of wind and deep circulation changes. *Geophys. Res. Lett.,* **43**, 1669–1678, https://doi.org/10.1002/2016GL067757.

Shatwell, P., A. Czaja, and D. Ferreira, 2020: Ocean heat storage rate unaffected by MOC weakening in an idealized climate model. *Geophys. Res. Lett.,* **47**, e2020GL089849, https://doi.org/10.1029/2020GL089849.

Shi, J.-R., S.-P. Xie, and L. D. Talley, 2018: Evolving relative importance of the Southern Ocean and North Atlantic in anthropogenic ocean heat uptake. *J. Climate,* **31**, 7459–7479, https://doi.org/10.1175/JCLI-D-18-0170.1.

Stocker, T. F., and S. J. Johnsen, 2003: A minimum thermodynamic model for the bipolar seesaw. *Paleoceanography,* **18**, 1087, https://doi.org/10.1029/2003PA000920.

Stommel, H., 1961: Thermohaline convection with two stable regimes of flow. *Tellus,* **13**, 224–230, https://doi.org/10.3402/tellusa.v13i2.9491.

Stouffer, R. J., 2004: Time scales of climate response. *J. Climate,* **17**, 209–217, https://doi.org/10.1175/1520-0442(2004)017<0209:TSOCR>2.0.CO;2.

Sun, S., and A. F. Thompson, 2020: Centennial changes in the Indonesian Throughflow connected to the Atlantic Meridional Overturning Circulation: The ocean's transient conveyor belt. *Geophys. Res. Lett.,* **47**, e2020GL090615, https://doi.org/10.1029/2020GL090615.

——, I. Eisenman, and A. L. Stewart, 2018: Does Southern Ocean surface forcing shape the global ocean overturning circulation? *Geophys. Res. Lett.,* **45**, 2413–2423, https://doi.org/10.1002/2017GL076437.

——, ——, L. Zanna, and A. L. Stewart, 2020a: Surface constraints on the depth of the Atlantic meridional overturning circulation: Southern Ocean versus North Atlantic. *J. Climate,* **33**, 3125–3149, https://doi.org/10.1175/JCLI-D-19-0546.1.

——, A. F. Thompson, and I. Eisenman, 2020b: Transient overturning compensation between Atlantic and Indo-Pacific basins. *J. Phys. Oceanogr.,* **50**, 2151–2172, https://doi.org/10.1175/JPO-D-20-0060.1.

Talley, L. D., 2013: Closure of the global overturning circulation through the Indian, Pacific, and Southern Oceans: Schematics and transports. *Oceanography,* **26**, 80–97, https://doi.org/10.5670/oceanog.2013.07.

Taylor, K. E., R. J. Stouffer, and G. A. Meehl, 2012: An overview of CMIP5 and the experiment design. *Bull. Amer. Meteor. Soc.,* **93**, 485–498, https://doi.org/10.1175/BAMS-D-11-00094.1.

Thompson, A. F., A. L. Stewart, and T. Bischoff, 2016: A multibasin residual-mean model for the global overturning circulation. *J. Phys. Oceanogr.,* **46**, 2583–2604, https://doi.org/10.1175/JPO-D-15-0204.1.

——, S. K. Hines, and J. F. Adkins, 2019: A Southern Ocean mechanism for the interhemispheric coupling and phasing of the bipolar seesaw. *J. Climate,* **32**, 4347–4365, https://doi.org/10.1175/JCLI-D-18-0621.1.

Viebahn, J., and C. Eden, 2012: Standing eddies in the meridional overturning circulation. *J. Phys. Oceanogr.,* **42**, 1486–1508, https://doi.org/10.1175/JPO-D-11-087.1.

Walczak, M. H., and Coauthors, 2020: Phasing of millennial-scale climate variability in the Pacific and Atlantic Oceans. *Science,* **370**, 716–720, https://doi.org/10.1126/science.aba7096.

Wang, G., S.-P. Xie, R. X. Huang, and C. Chen, 2015: Robust warming pattern of global subtropical oceans and its mechanism. *J. Climate,* **28**, 8574–8584, https://doi.org/10.1175/JCLI-D-14-00809.1.

Weijer, W., W. Cheng, O. Garuba, A. Hu, and B. Nadiga, 2020: CMIP6 models predict significant 21st century decline of the Atlantic meridional overturning circulation. *Geophys. Res. Lett.,* **47**, e2019GL086075, https://doi.org/10.1029/2019GL086075.

Winton, M., S. M. Griffies, B. L. Samuels, J. L. Sarmiento, and T. L. Frölicher, 2013: Connecting changing ocean circulation with changing climate. *J. Climate,* **26**, 2268–2278, https://doi.org/10.1175/JCLI-D-12-00296.1.

Wolfe, C. L., and P. Cessi, 2011: The adiabatic pole-to-pole overturning circulation. *J. Phys. Oceanogr.,* **41**, 1795–1810, https://doi.org/10.1175/2011JPO4570.1.

Xie, P., and G. K. Vallis, 2012: The passive and active nature of ocean heat uptake in idealized climate change experiments. *Climate Dyn.,* **38**, 667–684, https://doi.org/10.1007/s00382-011-1063-8.

Xie, S.-P., C. Deser, G. A. Vecchi, J. Ma, H. Teng, and A. T. Wittenberg, 2010: Global warming pattern formation: Sea surface temperature and rainfall. *J. Climate*, **23**, 966–986, https://doi.org/10.1175/2009JCLI3329.1.

Young, W. R., 2012: An exact thickness-weighted average formulation of the Boussinesq equations. *J. Phys. Oceanogr.*, **42**, 692–707, https://doi.org/10.1175/JPO-D-11-0102.1.